Sandra Grumm, BSc

A Study of Electrolyte Additives on High Voltage Cathodes in Lithium Ion Batteries

MASTER'S THESIS

to achieve the university degree of

Diplom-Ingenieurin

Master's degree programme: Technical Chemistry

submitted to

Graz University of Technology

Supervisor

Assoc. Prof. Dipl.-Chem. Dr.rer.nat. Bernhard Gollas
Institute for Chemistry and Technology of Materials

Dipl.-Ing. Dr. sc. ETH Stefan Freunberger
Institute for Chemistry and Technology of Materials

Graz, November and 2016

AFFIDAVIT

I declare that I have authored this thesis independently, that I have not used other than the declared sources/resources, and that I have explicitly indicated all material which has been quoted either literally or by content from the sources used. The text document uploaded to TUGRAZonline is identical to the present master‘s thesis.

_____ _____

Date Signature

Abstract

The aim of this work is to investigate the surface layer formation on $LiCoPO_4$ and $LiNi_{0.5}Mn_{1.5}O_2$ cathodes with and without additives in carbonate electrolytes. Therefore, five additives (succinic anhydride, glutaric anhydride, prop-1-en sultone, tris(trimethylsilyl)phosphate and tris(trimethylsilyl)borate) are chosen. The electrochemical performance of the cells is studied with galvanostatic and potentiostatic cycling as well as self-discharge experiments and the surface layer is scrutinized with online electrochemical mass spectrometry, infrared spectroscopy and nuclear magnetic resonance spectroscopy. For $LiNi_{0.5}Mn_{1.5}O_2$ as cathode materials especially the cells with anhydrides show an increase in coulombic efficiency and reduction in self-discharge in contrast to the base electrolyte. Thus, they might contribute the formation of the surface layer. Furthermore, through online electrochemical mass spectrometry and infrared spectroscopy investigations it is shown that salt decomposition is significantly contributing to surface layer formation and decreased by the addition of anhydrides for the $LiNi_{0.5}Mn_{1.5}O_2$ cathode. At high potentials the electrolyte degrades by forming carbonates that impact surface layer formation as confirmed by infrared spectroscopy and nuclear magnetic resonance investigations for both materials. For $LiCoPO_4$ as cathode material, only cells assembled with tris(trimethylsilyl)phosphate exhibit an increase in coulombic efficiency and a reduction in self-discharge and hence provide a positive influence in surface layer formation.

Kurzfassung

Ziel dieser Arbeit ist es die Bildung des Oberflächenfilmes von $LiCoPO_4$ und $LiNi_{0.5}Mn_{1.5}O_2$ Kathoden ohne und mit diversen Additiven in einem Carbonatelektrolyten zu untersuchen. Daher wurden fünf verschiedene Additive (Bernsteinsäureanhydrid, Glutarsäureanhydrid, Prop-1-ensulton, Tris(trimethylsilyl)phosphat und Tris(trimethylsilyl)borat) ausgesucht. Das elektrochemische Verhalten wurde mittels galvanostatischen und potentiostatischen Zyklen aber auch mit Selbstentladungsexperimenten analysiert. Der Oberflächenfilm wurde mittels online elektrochemischer Massenspektrometrie, Infrarotspektroskopie und Kernmagnetresonanzspektrospkopie untersucht. Im Falle des $LiNi_{0.5}Mn_{1.5}O_2$ Kathodenmaterials weisen vor allem die Zellen mit Anhydriden einen Anstieg in coulombscher Effizienz und eine Verringerung der Selbstentladung auf und tragen somit positiv zur Bildung des Oberflächenfilmes bei. Durch online elektrochemischer Massenspektrometrie und Infrarotspektroskopie wurde auf der $LiNi_{0.5}Mn_{1.5}O_2$ Kathode gezeigt, dass die Leitsalzzersetzung, welche einen Beitrag zur Filmbildung leistet, vor allem durch Anhydride verringert wird. An beiden Kathodenmaterialen wurde mittels Infrarotspektroskopie und Kernmagnetresonanzspektrospkopie bestätigt, dass es durch hohe Spannungen zu Elektrolytzersetzung unter Bildung von Carbonaten kommt, welche wiederum die Filmbildung beeinflussen. Im Falle des $LiCoPO_4$ Kathodenmaterials weisen nur Zellen mit Tris(trimethylsilyl)phosphat einen Anstieg in coulombscher Effizienz und eine Verringerung der Selbstentladung auf und tragen somit zur Bildung eines stabileren Oberflächenfilmes bei.

Acknowledgement

First of all I would like to give my sincere thanks to Dr. Stefan Freunberger for his support and supervision during my master thesis. Moreover, I want to thank Dr. Bernhard Gollas who allowed me to write my thesis under his supervision. Furthermore, I should express the warmest of thanks to Dipl.-Ing. Lukas Schafzahl. He always answered my questions and taught me necessary skills and knowledge for working with this matter.

I want to thank my working group, for informational support, help with the handling of new devices and a pleasant working atmosphere. Especially, I want to express gratitude to Dipl.-Ing. Bettina Schafzahl, who helped me with mass spectrometry. I want to thank Dr. Petra Kaschnitz, who helped me with NMR spectroscopy. I would like to give thanks to Dr. Chrisitan Slugovc for allowing me to use the FTIR device. Moreover, I want to acknowledge Christina Albering and Birgit Ehmann for providing me with chemicals and utensils.

I would like to give thanks to my office colleagues, who always cheered me up if experiments did not work the way they should and created a great working atmosphere. Furthermore, I want to express gratitude to my friends, who accompanied me during my studies and master thesis and helped me achieving it.

At last special thanks go to my boyfriend David, who always lend me an ear and granted me with proper motivation, my parents, whom without my studies would not have been possible and of course my sister and brother in law with their great support.

Table of Content

List of Figures

List of Tables

List of Schemes

List of abbreviations

CE	counter electrode
CV	cyclic voltammetry
DCM	dichloromethane
DMC	dimethyl carbonate
EC	ethylene carbonate
EIS	elechtrochemical impedance spectroscopy
EMC	ethylmethyl carbonate
FEC	flourethyl carbonate
FTIR	fourier transform infrared spectroscopy
GA	glutaric anhydride
HOMO	higherst occupied molecule orbital
LCP	$LiCoPO_4$
LFP	$LiFePO_4$
LiBOB	Lithium bis(oxalato)borate
LIBs	lithium ion batteries
LNMO	$LiNi_{0.5}Mn_{1.5}O_2$
LP30	EC: DMC 1:1 (m/m) and 1 M of $LiPF_6$
LUMO	lowest unoccupied molecular orbital
NMP	n-methyl-2-pyrrolidon
NMR	nuclear magnetic ressonance
OCV	open circuit voltage
OEMS	online elechtrochemical mass spectrometry
PC	propylene carbonate
PEC	polyethylene carbonate
PES	polyvinylidendifluoride
PS	propan sultone
PVDF	prop-1-en sultone
RE	reference electrode
RT	room remperature
RTIL	room temerature ionic liquids
SA	succinic anhydride
SEI	solid electrolyte interface
SL	surface layer
TFSI	bis(trifluoromethylsulfonyl)imide
TMSB	tris(trimethylsilyl)borate

TMSP	tris(trimethylsilyl)phosphate
VC	vinylene carbonate
WE	working electrode
XRD	X-ray Diffraction

1 Introduction

1.1 General

Lithium ion Batteries (LIBs) play a fundamental role in today's society. Therefore, a lot of research has been done over the last decades in modern electrochemistry.[1] In 1991 Sony reported the first Li-ion second generation battery with $LiCoO_2$ as cathode material[2]. It was eventually replaced by NMC (Li(Ni, Co, Mn)O_2) and $LiFePO_4$.[3,4] However, the quest for new cathode materials continues; $LiCoPO_4$ (LCP) or $LiNi_{0.5}Mn_{1.5}O_2$ (LNMO) have been proposed as high voltage materials.[5–8] They exhibit a discharge plateau of about 4.8 V vs. Li/Li^+. Due to their higher energy density they are very interesting for sustainable transportation like plug-in hybrid or full electric vehicles.[9]

Beside the cathode materials, electrolytes play a ubiquitous and fundamental part in electronic devices. The requirements for electrolytes are a large electrochemical potential, chemical inertness, low toxicity, high polarity (good conductivity) and inflammability. Conventional organic solvents are stable up to roughly 4.5 V vs. Li/Li^+ and thus, oxidize when the battery is charged up to 5 V vs. Li/Li^+.[10] The oxidation products contribute to the formation of a SL on the cathode. Due to the degradation of the electrolyte on the one hand investigations have been done for developing new electrolytes. For instance room temperature ionic liquids (RTIL), sulfones and dinitriles can be used as an electrolyte. Due to their high viscosity, low conductivity and inability of forming a proper SEI (solid electrolyte interface) on the anode they are however still not perfect for the usage in full cells. [11–14] On the other hand new additives have been proposed to contribute to the formation of the SL. Examples for such SL forming additives are anhydrides, sultones, phosphates and borates.[15–18] For the anhydrides Passerini and his group reported a diminution of self-discharge when adding succinic anhydride to the electrolyte.[19]

To fully rationalize the influence of additives and to further improve the electrolyte, a deeper understanding of the SL formation is needed. However, due to its complex composition and forming mechanism solving this puzzle remains challenging. Some pieces could be added by employing new instrumental approaches like online electrochemical mass spectrometry (OEMS) to investigate the gas formation during galvanostatic and potentiostatic cycling.[20–22] In this study, we want to investigate the influence and possible reaction mechanism of various additives on a LNMO and LCP cathode surface. For that purpose we chose succinic anhydride, glutaric anhydride, prop-1-en sultone, tris(trimethylsilyl)phosphate and tris(trimethylsilyl)borate to be added to a carbonate electrolyte (LP30, EC:DMC 1:1 1 M $LiPF_6$) (Figure 1).

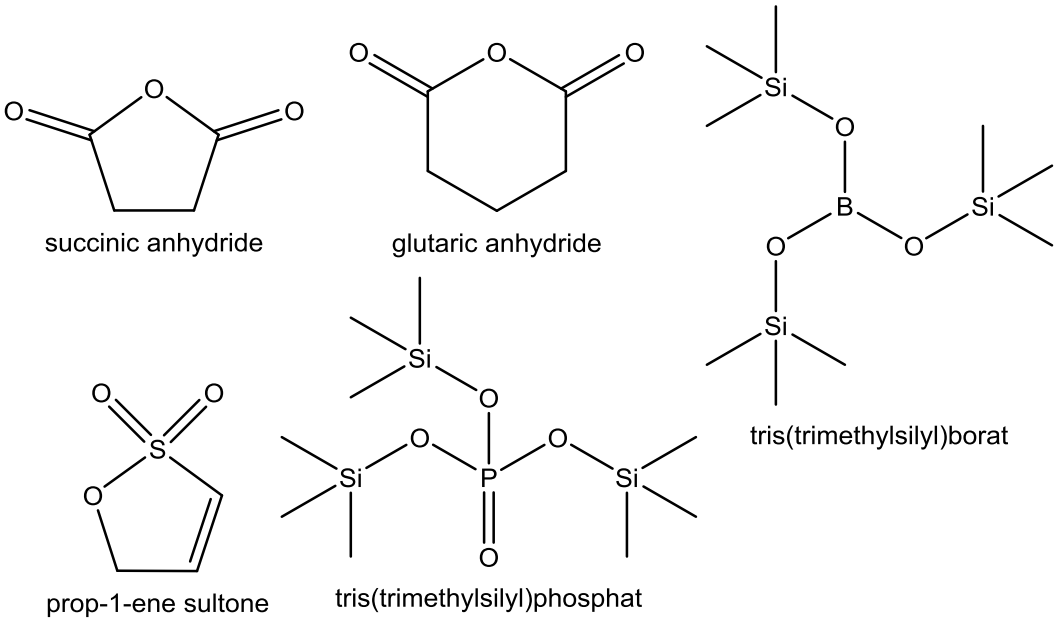

Figure 1: Additives used in LP30 electrolyte

1.2 High-voltage cathode materials

Currently used cathode materials ($LiCoO_2$, $LiFePO_4$) have discharge plateaus below 4.2 V vs. Li/Li^+ and an energy density of about 150 Wh/kg. However, $LiCoO_2$ has drawbacks due to its low energy density, high cost and safety concerns (toxicity of Co). LFP provides no safety concerns, but a low energy density.[23] Therefore, materials with larger capacities or higher discharge voltage platforms have been investigated to improve the energy density. Those cathode materials can be separated into three different groups: the polyanion, the lithium rich layered oxide and the spinel type cathode materials.[24] Due to the high discharge plateaus of some cathode materials these groups (greater than 4.5 V vs. Li/Li^+) are commonly termed high voltage cathode materials.

1.2.1 Polyanion cathode materials

Polyanion materials consist of a tetrahedral structure $(XO_4)^{n-}$, where X stands for P, S, As, Mo or W. [25] However, due to a difficult synthesis and infant research polyanion cathode materials are rarely reported. An exception are phosphates and fluorophosphates.[9]

The phosphates consist of an olivine type structure of $LiMPO_4$ (M = Fe, Mn, Co or Ni) that can be described as a slightly distorted hexagonal closed-packed (hcp), where oxygen forms the framework.[26] The metal atoms are located on each half of the octahedral sites and the phosphor atoms at $^1/_8$ of the tetrahedral sites as shown in Figure 2.[25] $LiFePO_4$ is a widely studied compound among the phosphates. However, due to its low flat voltage of 3.4 V vs. Li/Li^+ [26], it does not classify as high voltage cathode material. In contrast $LiCoPO_4$ and $LiNiPO_4$ show a high flat voltage plateau at 4.8 V and 5.1 V vs. Li/Li^+, respectively.[27–29] $LiCoPO_4$ has an energy density of approximately 800 Wh/kg. Thus, it is a promising candidate among olivine phosphates. A drawback is the low electronic conductivity, because of a one-dimensional (1 D) ion transport channel.[25] To increase the conductivity several methods were applied like modifying the surface, doping with metal ions and decreasing the particle size.[30–32]

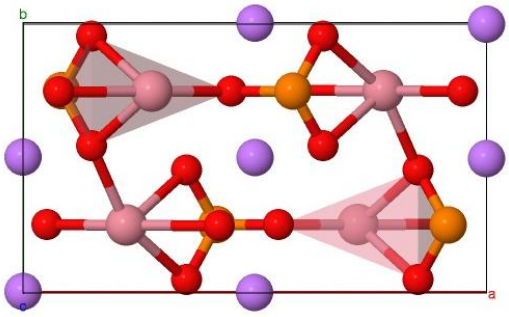

Figure 2: $LiMPO_4$; magenta (Li), pink (M), red (O), orange (P) [25]

$LiCoPO_4$ charges and discharges over a two-phase reaction in a three phase system. [33]

$$LiCoPO_4 \rightarrow Li_{0.6}CoPO_4 + Li_{0.4}^+ \rightarrow CoPO_4 + Li$$

The intermediate phase $Li_{0.6}CoPO_4$ is formed upon delithation and then transformed to $CoPO_4$. The complete delithated compound is very unstable at room temperature and changes to the amorphous form.

$LiNiPO_4$ has been very scarcely tested due to its high redox potential. At high voltages the nowadays available electrolytes are not stable and decompose. Thus, the application of $LiNiPO_4$ relies on the development of new electrolytes.[25]

This also holds true for fluorophosphates that are possible high voltage materials due to the inductive effect of the PO_4^{3-} group and high electronic negativity (F^-). The general sum formula is A_2MPO_4F (A = Na, Li; M = Co, Ni, Fe, Mn), but three different crystalline structures exist;[34–36] a layered (e.g. Na_2FePO_4F), stacked (e.g. Li_2CoPO_4F) or 3 D (e.g. Na_2MnPO_4F) structure is possible.[37]

The first reported fluorophosphates phase, which was capable of lithium ion insertion/extraction is $LiVPO_4F$.[38–40] It is build-up of a 3 D network and reaches a capacity of 155 mAh/g.[41] Proposed potential cathode materials are Li_2CoPO_4F[42] and Li_2NiPO_4F[43] with discharge plateaus of 5.0 V vs. Li/Li^+ and 5.3 V vs. Li/Li^+, respectively.[25]

1.2.2 Li-rich layers oxide cathode materials

A well known Li-rich layered oxide material is $LiCoO_2$. As mentioned before, due to its low energy density, safety issues and high costs the application in electric and hybrid vehicles is useless. Through the introduction of Ni or Mn by forming a ternary composition of $LiNi_{1/3}Mn_{1/3}Co_{1/3}O_2$, cost is reduced and safety improved, but the energy density remains similar.[44]

However, a solid solution of $xLi_2MnO_3{\cdot}(1\text{-}x)LiMeO_2$ (Me = Ni, Co, Mn) attains a discharge voltage of 3.5 V vs. Li/Li^+ and a discharge capacity over 300 mAh/g can be reached when cycled between 2.0 and 4.8 V vs. Li/Li^+. Below 4.5 V vs. Li/Li^+ Ni(II) and Co(III) oxidize to Ni(IV) and Co(IV). Above this voltage the valence of Mn is not changing, but a structural distortion takes place. This leads after several cycles to an irreversible capacity.[45] Attempts have been made to decrease the irreversible capacity (e.g. acid treatment, doping and coating).[46, 47, 9] Through surface modification via coating the cycling stability as well as the rate performance is improved.[47] However, still the poor rate performance is the limiting factor of Li-rich layered oxides.

1.2.3 Spinel type materials

One of the most popular spinel type materials is $LiMn_2O_4$. In addition to its low cost and environmental friendliness, it provides a 3 D Li^+ diffusion pathway and thus reaches a high rate capability.[9] Drawbacks are capacity fading due to irreversible structural transition from spinel to tetragonal structures. This happens because of the Jahn-Teller effect (distortion of Mn(III)) and dissolution of Mn ions into the electrolyte.[9]

To overcome those problems Mn can be doped with other metals (e.g. Ni, Mg, Ti, Fe, Co, Zn, Cu, Nb).[9,48–51] This suppresses the Jahn-Teller effect and the cycling stability is improved. A widely investigated cathode material is $LiNi_{0.5}Mn_{1.5}O_4$ (LNMO). For this material two crystal structures (Figure 3) are possible, whereof one is stoichiometric ordered ($P4_332$ space group) and the other one is non-stoichiometric disordered ($Fd\bar{3}m$ space group). The second structure is favored due to its higher electronic conductivity and thus better rate capability.[52]

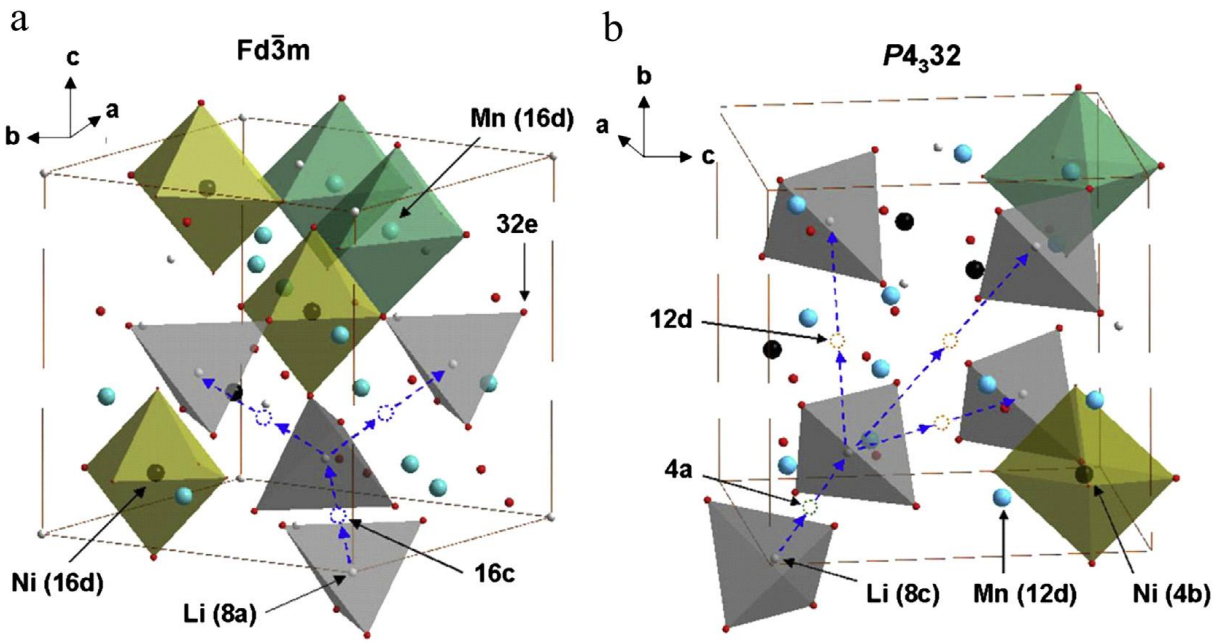

Figure 3: LNMO structure; (a) non-stoichiometric disordered; (b) stoichiometric ordered[52]

LNMO provides a theoretical capacity of 147 mAh/g. At 4 V vs. Li/Li^+ Mn(III) oxidizes to Mn(IV) and at 4.7 – 4.75 V vs. Li/Li^+ the oxidation of Ni(II) over Ni(III) to Ni(IV) occurs.[53] Passerini et al. reported that the charge discharge coulombic efficiency is 94 % after the first cycle and after the 3rd cycle it reaches 97 % at C/10.[53] At higher voltages the electrolyte decomposes and generates a thick surface layer. To decrease this problem the surface of the cathode was coated (e.g. ZnO, Al_2O_3, Ag, Au).[45,54,55] However, some coating materials hinder the Li^+ transfer between the electrolyte and the electrode. In contrast, nanoparticles

improve the rate capability due to shorter diffusion pathways, but aggravate electrolyte decomposition due to their higher surface area.

1.3 Electrolytes

Electrolytes are vital for cell performance. The solvents should be polar enough to dissociate the conducting salt and electrochemically inert to obtain a large electrochemical window.[56] The thermodynamic stability of the electrolyte is limited by its HOMO (highest occupied molecule orbital) and its LUMO (lowest unoccupied molecule orbital) (Figure 4[57]). If the potential of the cathode is below the HOMO of the electrolyte, an oxidation occurs that leads to electrolyte degradation.

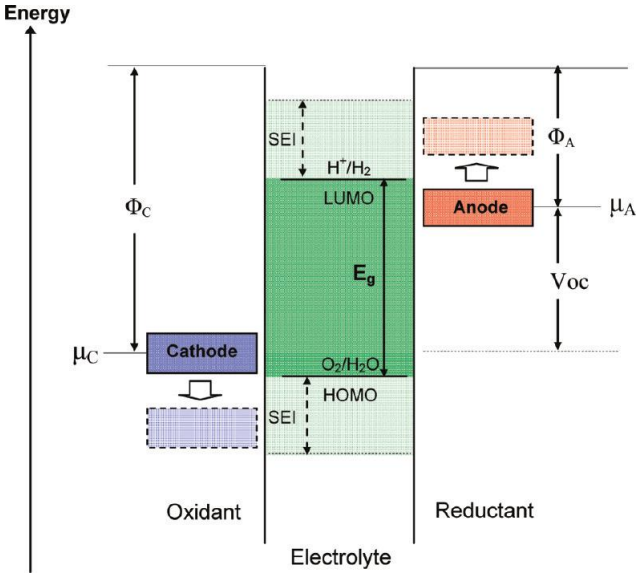

Figure 4: Schematic open-circuit energy diagram with aqueous electrolytes Φ_A and Φ_C and the thermodynamic stability of the electrolyte (E_g) (illustration taken form Goodenough et al.[57])

This is the case for high voltage cathodes materials. Hence, the degradation of the electrolyte is the core issue in the field of high voltage batteries. Thus, alternative solvents have been proposed which should decrease the electrolyte oxidation.[24]

1.3.1 Solvents

Room temperature ionic liquids (RTIL) provide a large electrochemical window and thus are candidates for electrolytes in high voltage batteries.[11] Moreover, they boast a high thermal stability, low flammability and low volatility. They are usually quaternary ammonium salts such as for instance imidazolium, piperidinium or pyrrolidinum salts. Sulfonium as well as

phosphonium cations are also known to be RTIL. For the 1-alkyl-3-methylimidazolium tetrafluoroborat the anodic limit lies at about 5 V vs. Li/Li^+. However, the cathodic limit is at about 1 V vs. Li/Li^+ which leads to a cation decomposition at the anode.[12] It should be taken into account that the kind of anion plays an important role for electrochemical stability. Gerbrand et al. calculated the stability limits of 1-butyl-3-methylimidazolium with different anions (PF_6^-, BF_4^-, bis(trifluoromethylsulfonyl)imide (TFSI)) with a combination of molecular dynamics simulations and density functional theory.[58] BF_4^- provides the highest and TFSI the lowest anodic limit with a potential of 6.92 V vs. Li/Li^+ and 6.63 V vs. Li/Li^+, respectively. Pyrrolidinium salts exhibit an electrochemical window range of above 5 V with higher reduction and oxidation limits than imidazolium salts. Furthermore, it provides a higher conductivity (> 10^{-3} S/cm), Li^+ transference number (about 0.4) and lower viscosity as the imidazolium salt. In addition at long rate cycling the formation of dendrite lithium can be suppressed.[59–61] However, the only reported RTIL successfully cycled with an graphite anode was 1-methyl-1-propyl pyrrolidinum bis(fluorosulfonyl)imide as electrolyte containing LiTFSI as salt. It reached a specific capacity of 340 mAh/g for over 100 cycles and a coulombic efficiency of above 70 %.[62] Additional drawbacks of RTIL are its low ionic conductivity and high viscosity which results in poor cycling stability and rate performances.

Another class of possible solvents for electrolytes in high voltage batteries are sulfones due to their high dielectric permittivity, low flammability and good anodic stability. The oxidation potential lies at about 5.5 V vs. Li/Li^+.[13] Due to their inability of forming a stable SEI on the graphite surface, they are not practicable as a sulfone based electrolyte. To overcome this issue, surface forming additives, like vinylene carbonate (VC), lithium difluoro(oxalate)borate or hexamethylene diisocyanate have to be added to a sulfone based electrolyte.[63–65] Moreover, co-solvents can be used to improve conductivity and wettability and decrease the viscosity.[66]

Aliphatic dinitrile based electrolytes provide a good electrochemical stability and a large electrochemical window. Thus, they are another promising candidate for high voltage cathode materials. Glutaronitrile for example, exhibits an electrochemical potential over 6 V with an anodic limit of approximately 8 V vs. Li/Li^+.[14] However, due to their poor compatibility with both Li metal or graphite anode and easy reduction, co-solvents and additives need to be added to the aliphatic dinitrile based electrolyte. A possible solvent and additive system are ethylene carbonate (EC) and Lithium bis(oxalate)borate (LiBOB), respectively. They help forming a proper SEI on the anode and hence allows a reversible Li^+ insertion/extraction.[67] Adiponitrile provides almost the same properties as gluraronitrile. The electrochemical

window ranges over 6 V. However, co-solvents and co-salts needs to be added to gain a reversible cell performance.[68]

Although dinitrile based electrolytes, sulfone based electrolytes and RTIL exhibit a large electrochemical window, they suffer from high viscosity, low conductivity and inability of forming a stable SEI for Li^+ insertion/extraction. Thus, additives need to be added to improve the cell performance. Hence, organic electrolyte solvents like EC and DMC are widely used in combination with high voltage cathode materials.[16,20,53] They provide low toxicity, acceptable safety features and high polarity.[10] Due to the formation of an unstable SL on the cathode, additives need to be added to the electrolyte.[69]

1.3.2 Cathode/Electrolyte interphase

The interphase is formed on the surface of an electrode and thus separates the electrolyte from the electrodes. The cathode/electrolyte interface is called SL. The interphase formation of the cathode can be assumed to take at least three steps. At first, a native surface film forms during electrode manufacturing. Secondly, spontaneous reactions result in formation of Li_2CO_3, LiF, PO_xF_v due to the exposure of the native film with the electrolyte. Li_2CO_3 is formed due to the reaction of CO_2 with Li_2O. LiF and CO_2, in turn, are formed from HF originating from the PF_6 anion. At last during initial charging an electrochemical rearrangement takes place.[56] Commonly used organic electrolytes consist of EC/DMC or EC/DEC. Due to the higher dielectric constant of EC, those molecules have a stronger tendency to adsorb on the cathode surface and to solvate Li^+ ions. Hence, EC is preferentially oxidized.[70] Until 4.5 V vs. Li/Li^+ carbonate electrolytes are relatively stable, but above this voltage oxidation/decomposition is occurring.[71] Xing et al. theoretically investigated the oxidative stability of EC in high voltage LIBs. He proposed that a radical cation $EC^{\cdot+}$ is generated after transferring one electron on the cathode surface. Five decomposition mechanism of the radical (Figure 5) are possible, whereof the formation of CO_2 and 2-methyl-1,3-dioxolane is the most favorable one.[72]

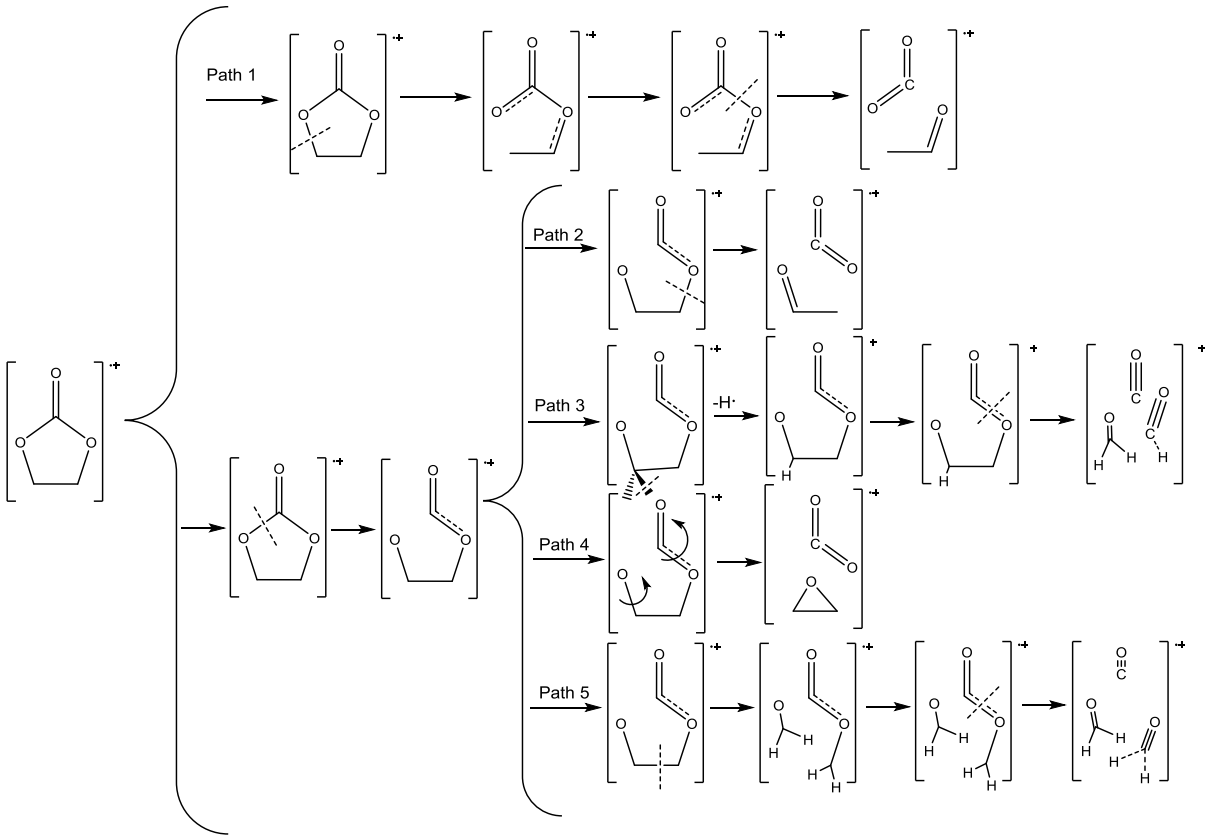

Figure 5: Possible degradation pathways of EC[72]

Yang et al. found characteristic adsorption peaks via FTIR analysis consisting of, amongst other things, poly(ethylenecarbonate) (PEC).[73] Moreover, Dedryvére et al. revealed the domination of more organic species rather than lithiated salt species.[74] Besides that, Murakami et al. confirmed that at potentials higher than 4.9 V vs. Li/Li^+ fluorides like LiF were produced.[75]

In summary, the formation of the surface layer is a complex process and yet not fully understood. In a typical carbonate mixture, EC is oxidized above 4.5 V vs. Li/Li^+, which leads to the formation of CO_2, oxalane and PEC. Unfortunately, these products do not fully passivate the cathode resulting in continuous electrolyte decomposition and poor cycling stability. Therefore, various additives were envisioned to stabilize the cathode/electrolyte interface.

1.3.3 Additives

The formation of the SL plays an important role in cell performance. Thus, additives with a HOMO level higher than of the organic solvents need to be added to the electrolyte to overcome electrolyte degradation.[9,73]

1.3.3.1 Anhydrides

Lee et al. reported that the addition of succinic anhydride (SA) (Figure 6) and 1,3-propane sultone (PS) to LP30 electrolyte of a LNMO/Graphite cell benefits the formation of a stable SEI on the anode during the first Li-intercalation process. As no oxidative decomposition of SA was observed up to potentials of 6 V on a platinum anode, no beneficial influence of this anhydride for a cathode was assumed.[15] However, Passerini and his group confirmed the favorable influence on a cathode. Due to SA, a thinner more stable SL on the LNMO cathode is formed. Hence, better cell performance was achieved with coulombic efficiencies of 99.6 % (base electrolyte 99.4 %). Additionally, the self-discharge was decreased by 50 % and salt decomposition reduced with fluorophosphates ($Li_xPF_yO_z$) being the favored oxidation product instead of LiF.[19] Another anhydride providing beneficial influence on the cell performance is glutaric anhydride (GA) (Figure 6). The self-discharge over two weeks is reduced from 28 % to 16 %. Moreover, the capacity fading decreases from 25 % to 15 % after 120 cycles. Bouayad et al. showed that the SL on the cathode is thicker, but more conductive.[76] Moreover, the additives exhibit a good influence on salt degradation since less LiF and more fluorophosphates are formed. This indicates a reduced salt degradation.

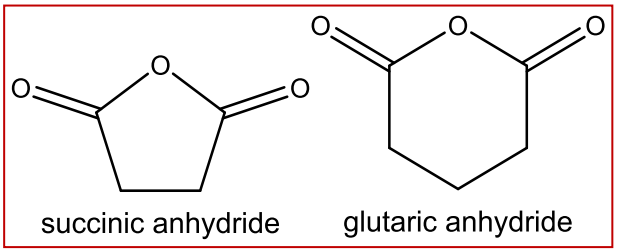

Figure 6: Structure of the anhydrides

1.3.3.2 Sultones

Another promising group of additives are the sultones (Figure 7). Li et al. reported that pro-1-ene-1,3-sultone has a beneficial influence on the formation of the SEI on anodes. It exhibits a better cycling stability and less capacity loss than propylene carbonate (PC).[77] Moreover, Dahn and his group showed that the addition of PES in a $Li(Ni_{1/3}Mn_{1/3}Co_{1/3})O_2$/Graphite pouch cell provides a stronger effect on coulombic efficiency and charge transfer resistance than vinylene carbonate (VC). In fact, the interface impedance is increased at the negative electrode and decreased at the positive electrode.[78]

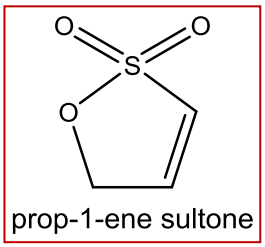

Figure 7: Structure of the sultone

1.3.3.3 Borates and Boroxines

Lithium bis(oxalato)borate (LiBOB), (Figure 8) which also stabilizes the graphite anode, is a commonly used additive in high voltage batteries. Dalavi et al. observed an improve in capacity retention, coulombic efficiency and decrease of impedance for LNMO cathodes.[79,80] However, the olivine $LiCoPO_4$ cathode material still suffers severe problems with fast fading capacity.[81] Lithium difluoro(oxalato)borate was found to be another borate additive which favors the formation of a stable surface layer formation, reducing electrolyte degradation.[82] Horino et al. investigated boroxines with different substituents. He found that resistance decreases with increasing chain length. Tris-isopropoxy boroxine provided the best cell performance. Moreover, the anodic stability of the carbonate electrolyte was improved up to 5 V vs. Li/Li^+.[83] Dahn and his group investigated that by adding 0.3 % and 1.0 % trimethoxy boroxine to the electrolyte a decrease in the cells impedance is occurring.[84] Another promising additive is trimethylboroxine. Shrabi et al. investigated this additive in FEC-based electrolytes on $LiCoPO_4$. It provided good cycling performances with a capacity retention of 90 % and with a faradaic efficiency of 98 %.[85]

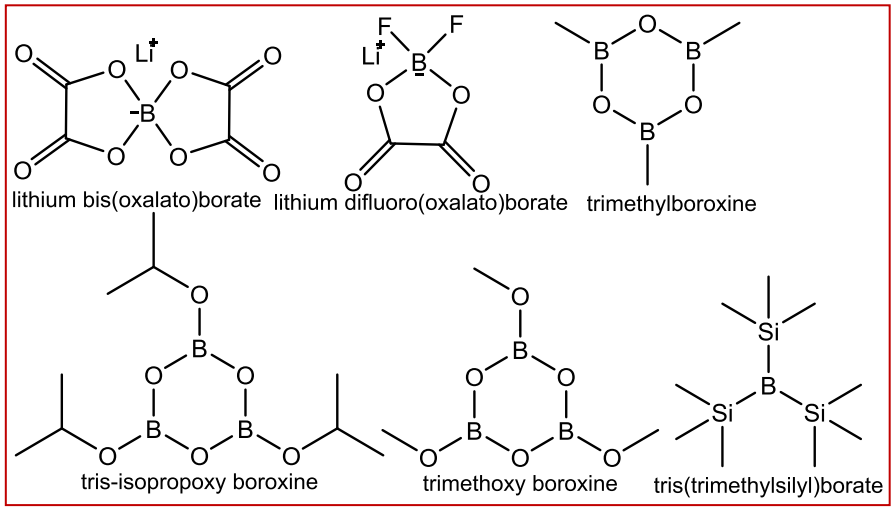

Figure 8: Structures of borate and boroxine additives

Zuo et al. investigated the film formation of TMSB in an ethylene carbonate (EC) and ethyl methyl carbonate (EMC) (1:2) with 1 M $LiPF_6$ electrolyte on a $LiNi_{0.5}Co_{0.2}Mn_{0.3}O_2$ cathode. They investigated improved capacity retention when cycled between 3.0 - 4.4 V. Furthermore, they discovered a thinner SL, which protects EC from decomposition.[86]

1.3.3.4 Phosphorous based additives

Tri(hexafluoro-iso-propyl)phosphate (Figure 9) is a phosphorous based additive which provides improved anodic stability and cycling performance. It exhibits capacity retention of 72.3 % after 130 cycles (reference 64.5 %). Moreover, the impedance is minimized and the reversible cycling is extended on a LNMO cathode.[71,87] Xu et al. investigated tris(pentafluoophenyl)phosphine (Figure 9) in an organic solvent on LNMO electrode. It improves cycling performance due to the formation of a protective film on the cathode. The additive tends to be preferably oxidized and thus the decomposition of the electrolyte is reduced.[88]

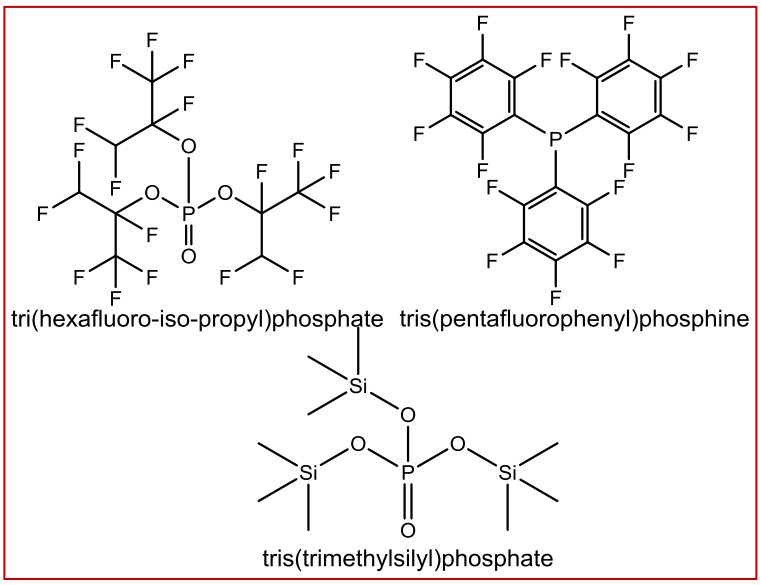

Figure 9: Structure of the phosphorous based additives

Yan et al. investigated the influence of TMSP in a $LiPF_6$ based organic electrolyte on a $LiNi_{0.5}Co_{0.2}Mn_{0.3}O_2$ cathode. They discovered improved cycle performance when cycled between 3.0 and 4.5 V (vs. Li/Li^+). TMSP decomposes before the organic electrolyte and thus contributes to the formation of SL. Electrochemical impedance spectroscopy (EIS) measurements exhibits a decrease in interface impedance. Furthermore, through TEM and XPS measruemets they confirm that the formed SL leads to a better protection of the $LiNi_{0.5}Co_{0.2}Mn_{0.3}O_2$ cathode from HF corrosion.[89]

Many additives were shown to improve cell performance for high-voltage electrodes. However, these results are hard to compare due to deviating experimental conditions, electrode materials and preparation, electrolyte composition and additive ratios. In this study, SA, GA, PES, TMSB and TMSP were chosen as representative additives from these groups and compared under identical conditions. Then the SLs formed by these additives were investigated.

1.4 Recent investigations in online electrochemical mass spectrometry (OEMS)

Many methods have been employed to investigate the surface layer and its formation on the cathode. *Ex-situ* measurements like FTIR or NMR are proper methods to gain information of the composition of the SL. However, with *in-situ* measurements like OEMS information on the reaction mechanism due to gas evolution during cycling can be explored. This helps in understanding the influence of the electrolytes and additives contributing to the SL.

Berg et al. compared the solvent influence of a LP30, DMC and EC electrolyte and the salt influence of LP30 and LC30 (EC:DMC 1:1 1 M $LiClO_4$), respectively. CO_2, CO, H_2 and POF_3 are volatile species displaying a systematic trend during charge and discharge. For EC, DMC and LP30, a CO_2 evolution appears at a voltage of 4.6 V vs. Li/Li^+ and in the range between 4.7 and 5.0 V vs. Li/Li^+. The first peak is related to the formation of a passivation layer, whereas the second peak corresponds to the anodic oxidation of the carbonate solvent. When the concentration of Ni(III) reaches its maximum, the lowest evolution of CO_2 is observed. Thus, the oxidation state of the Ni ion plays a role in the electrolyte decomposition. The formation of POF_3 relates to the CO_2 evolution during discharge. H_2 is formed by the reduction of H_2O on the Li metal counter electrode. CO evolution is observed at the beginning and almost at the end of the charging process. The comparison of LC30 and LP30 reveals a similar pattern in the evolution of CO_2, H_2 and CO. However, with $LiClO_4$ as conducting salt, CO_2 evolution increases drastically. Due to the absence of $LiPF_6$ in LC30 no evolution of POF_3 is exhibited.[20]

Berg et al. investigated the gas evolution of EC or FEC based electrolyte on a NMC full and half cell via OEMS. The evolution of CO_2 was reported at 4.2 V vs. Li/Li^+ and at voltages higher than 4.5 V vs. Li/Li^+. They both belong to the Li_2MnO_3 domain activation. The formation of POF_3 was found in every setup except in a graphite /Li half cell. They concluded that anodic polarization is needed for the formation. The formation mechanism of POF_3 suggested by Tasaki et al. includes CO_2 evolution. [90]

$$Li_2CO_3 + LiPF_6 \rightarrow 3\ LiF + POF_3 + CO_2$$

$$Li_2CO_3 + PF_5 \rightarrow 2\ LiF + POF_3 + CO_2$$

As Li_2CO_3 formation is reduced in an EC:DEC electrolyte, less POF_3 is formed.[21]

Guéguen et al. investigated the decomposition of $LiPF_6$ via OEMS. He concluded that carbonate solvent oxidation appears at voltages higher than 4.2 V vs. Li/Li^+ under formation of reactive species (e.g. ROH). Those alcohols hydrolyze the conducting salt to form POF_3. He proposed a schematic loop shown in Figure 10.

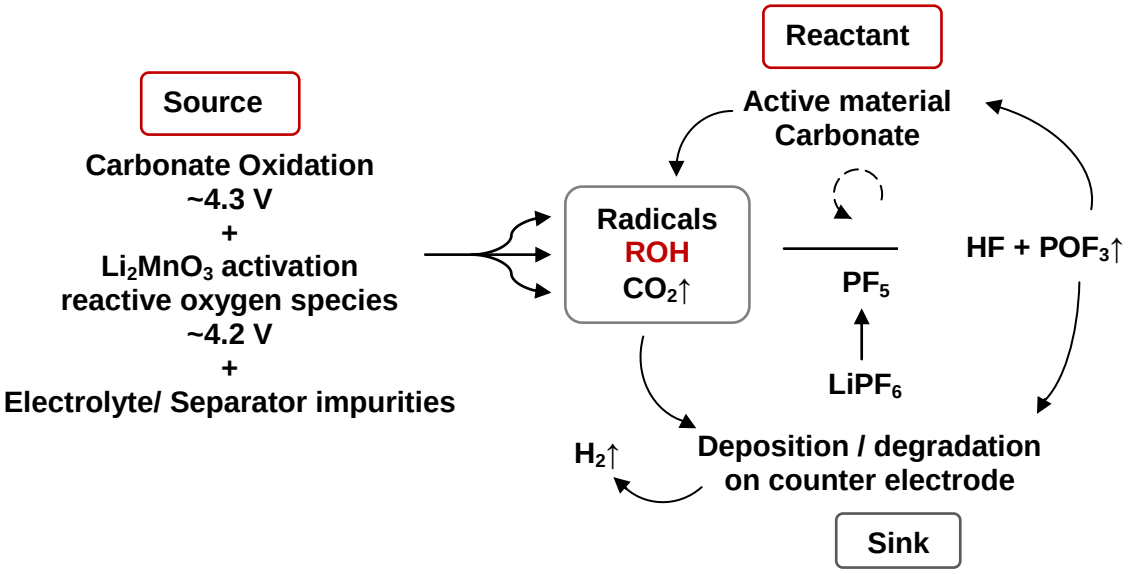

Figure 10: Schematic loop (illustrated by Guéguen et al.) representing involved reactants and formed products in POF_3 formation.[22]

Furthermore, he investigated that surface and glass fiber impurities lead to increase in the formation of POF_3.[22]

In summary, OEMS is a powerful method for the investigation of the decomposition mechanism of the electrolyte. In general four different volatile substances (CO_2, CO, H_2 and POF_3) are of main interest and play an important role in the electrolyte oxidation. However, until now only a few insights in gas evolution during cycling have been documented and thus leaves room for further investigations.

1.5 Aim of this work

The aim of this work is on the one hand to investigate the surface layer formation on LCP and LNMO cathodes with carbonate electrolytes containing additives and no additives. On the other hand the electrochemical performance of cells with carbonate electrolytes containing additives and no additives are tested. The five additives (succinic anhydride, glutaric anhydride, prop-1-en sultone, tris(trimethylsilyl)phosphate and tris(trimethylsilyl)borate) are chosen due to their before mentioned beneficial influence in cell performance. The electrochemical performance of the cells is studied with galvanostatic and potentiostatic cycling as well as self-discharge experiments and the surface layer is scrutinized with OEMS, fourier transform infrared spectroscopy (FTIR) and nuclear magnetic resonance spectroscopy (NMR).

2 Results and Discussion

2.1 Stability of the additives

The anodic stability of additives succinic anhydride (SA), glutaric anhydride (GA), prop-1-en sultone (PES), tris(trimethylsilyl)phosphate (TMSP) and tris(trimethylsilyl)borate (TMSB) were investigated by cyclic voltammetry (CV). In high voltage batteries the cathode material requires charging up to a voltage of 5 V vs. Li/Li$^+$. Since the base electrolyte is not stable enough and starts being oxidized, a SL on the cathode is formed, resulting in a positive current. Additives should add to this current as they need to decompose to effect SL formation. Ideally, they would be less stable than the electrolyte to be oxidized preferentially.

The stability of the additives was first investigated with glassy carbon as working electrode. To differentiate additive oxidation from solvent oxidation the measurements were done in MeCN as solvent, which has a higher oxidative stability than the carbonates. An increase in the current density below 5 V vs. Li/Li$^+$ was expected. However, the current density of the cell containing SA, GA or PES decrease compared to base electrolyte as shown in Figure 11 (a). This was expected for the cell containing SA, as Lee et al reported a higher stability of SA.[15]

In contrast, the cells with the electrolyte containing silyladditives show current densities above the base electrolyte and the additives participated in SL formation as shown in Figure 11 (b). TMSP starts to oxidize at 4.9 V vs. Li/Li$^+$. At 5.5 V vs. Li/Li$^+$ another increase in current density take place. TMSB first reacts at 3.5 V vs. Li/Li$^+$ and then at 5.5 V vs. Li/Li$^+$.

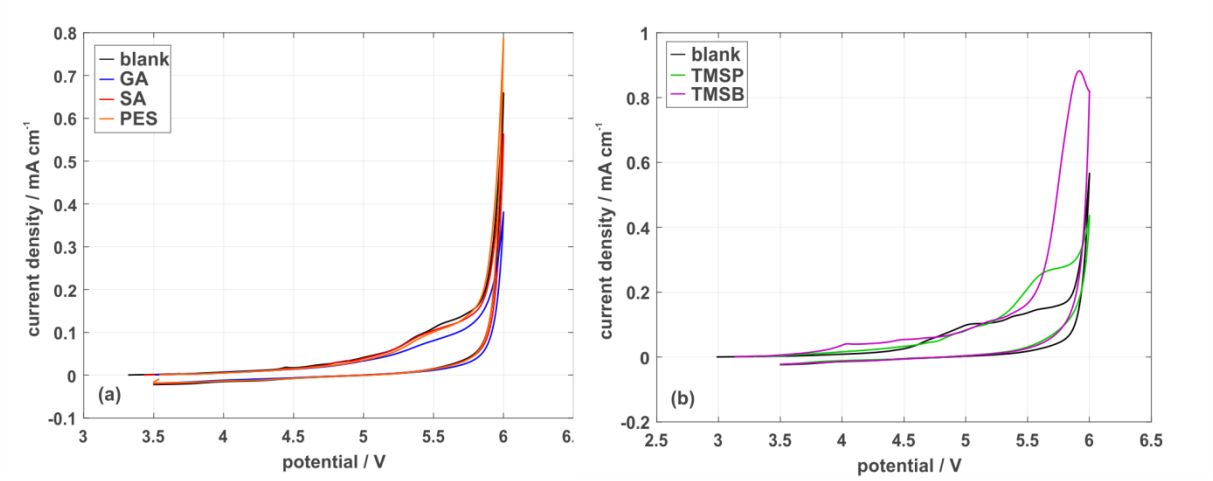

Figure 11: Cyclic voltammograms at 100 mV/s in a MeCN electrolyte with 0.1 M $LiClO_4$ and 2 wt.% of SA, GA, PES (a) and TMSP and TMSB (b). Three electrode configuration with glassy carbon as WE (diameter 3 mm), LFP on a syringe needle as RE and CE.

Since the additives on glassy carbon exhibited no drastic increase in anodic current, the stability of the additives could depend on the cathode material. Hence, it was further tested on LNMO and conductive carbon black (SuperP). As expected, in contrast to glassy carbon as working electrode, the coated electrodes showed much higher reactivity. The LNMO coated glassy carbon electrode shows the oxidation of Mn(II) to Mn(III) at 4.0 V vs. Li/Li^+. At 4.8 V vs. Li/Li^+, an increase in current density occurs, which corresponded to the oxidation of Ni(II) to Ni(IV).

In Figure 12 (a) the 1st cycle of the cell containing SA is shown. It exhibits a higher current density starting at 4.6 V vs. Li/Li^+ for LNMO and SuperP, respectively. This indicates an oxidation of the additive. On SuperP two peaks in current density are visible. For the cell containing GA, the current density on LNMO increases only slightly. However, on SuperP a strong increase in current density appears at 4.7 V vs. Li/Li^+ (Figure 12 (b)).

As shown in Figure 12(c)/ (d) cells containing TMSP or TMSB exhibit a higher reactivity, if only SuperP is present. This could be due to the higher amount of conductive black carbon, which leads to an increased surface area and increase in total oxidation. Besides the higher surface and thus higher reactivity, the cells containing silyladditives show the same oxidative behavior as with the blank glassy carbon electrode. The cell with the electrolyte containing PES additive (Figure 12(e)) shows drastically higher current densities on SuperP. For the LNMO coating a slight increase in current density starts at 4.8 V vs. Li/Li^+.

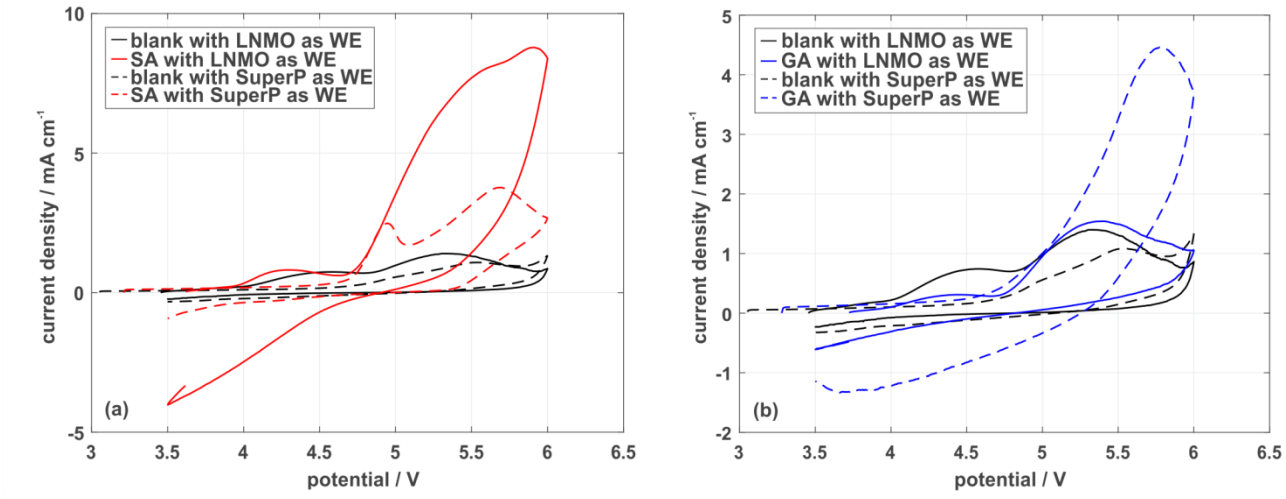

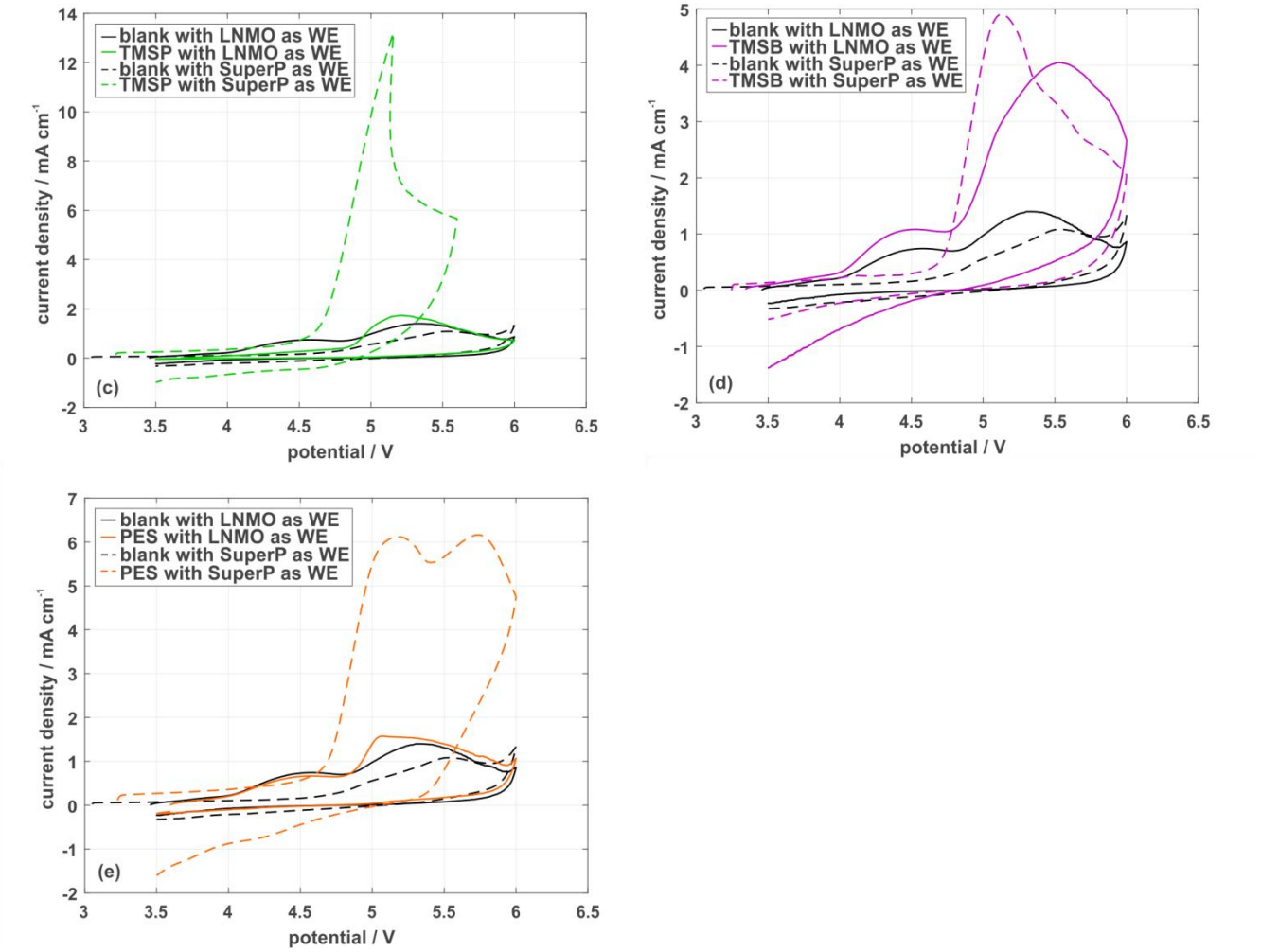

Figure 12: Cyclic voltammograms at 100 mV/s consisting of MeCN electrolyte 0.1 M LiClO4 and 2 wt.% additives. Dashed line refers to SuperP and full line to LNMO.

On carbon black the reactivity is increased due to the higher surface area. On glassy carbon, only the cells containing the silyladditives show an inrease in current density. The increase in current density of the cells containing anhydride additives appear always at the same voltage for LNMO and SuperP. In the presence of glassy carbon no increase is present. The cell containing PES exhibits a high increase in current density in the presence of SuperP, but only a slight on LNMO and non on glassy carbon (Figure 13).

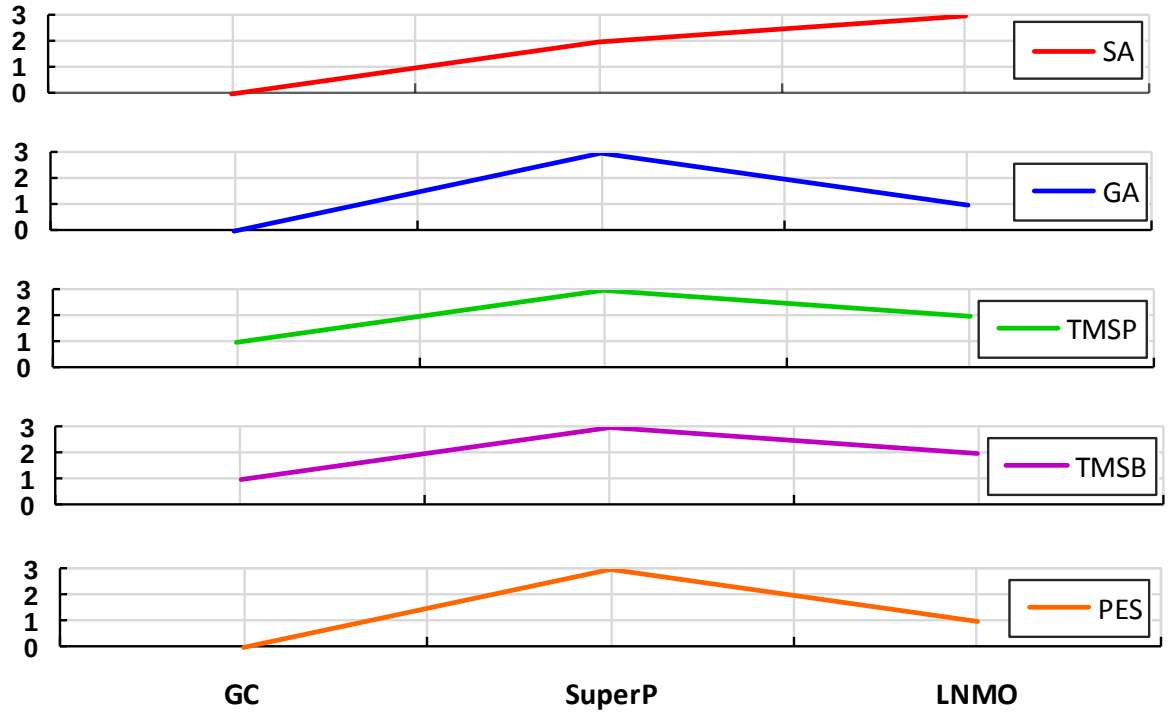

Figure 13: The reactivity intensities varied from 0 (inferior) to 3 (best) of the additives on different surfaces.

2.2 Investigation of the cathode LNMO material

2.2.1 Spinel type LNMO cathode material

LNMO_SG was prepared by S. Brutti et al. via sol gel and LNMO_WC via wet chemistry synthesis.[6] Due to different synthesis methods, the electrodes show different behavior in CV as well as in cycling tests.

For electrodes prepared from LNMO_SG electrodes the CVs seemed less reproducible as compared to LNMO_WC. Figure 14 presents the CVs of each synthesis method. At about 4 V vs. Li/Li^+ the oxidation of Mn(III) to Mn(IV) occurs.[53] The oxidation of Ni(II) to Ni(IV) starts at about 4.8 V vs. Li/Li^+.[53] For the LNMO_WC electrodes, two peaks are clearly visible in this area referring to a two-step oxidation of the nickel ion. This oxidation is not clearly visible for the LNMO_SG electrode.

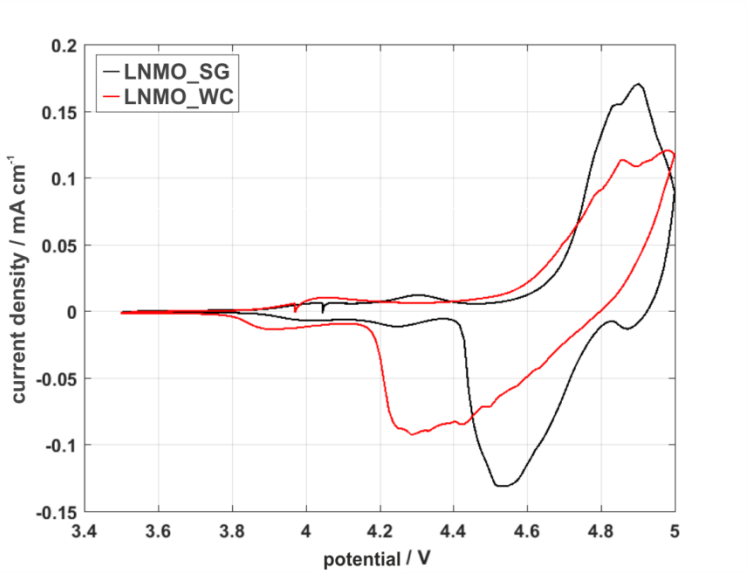

Figure 14: Cyclic voltammograms at 0.05 mV/s used an EC:DMC (1:1) 1 M $LiPF_6$ electrolyte. Black line represents LNMO_SG and red line LNMO_WC.

Figure 15 shows the specific capacity and columbic efficiency of the two different LNMO cathode materials. A decrease in specific capacity is visible in each cell. However, LNMO_SG initially provides a much higher specific capacity (126 mAh) than LNMO_WC (116 mAh). In contrast, LNMO_WC provides a higher coulombic efficiency (CE) (96 %) than LNMO_SG (94 %). Nonetheless, all cells show good cycling performance over 50 cycles, without drastic capacity fading or low CEs. Note that in the 6th cycle the resting period for self-discharge deteriorates the coulombic efficiency.

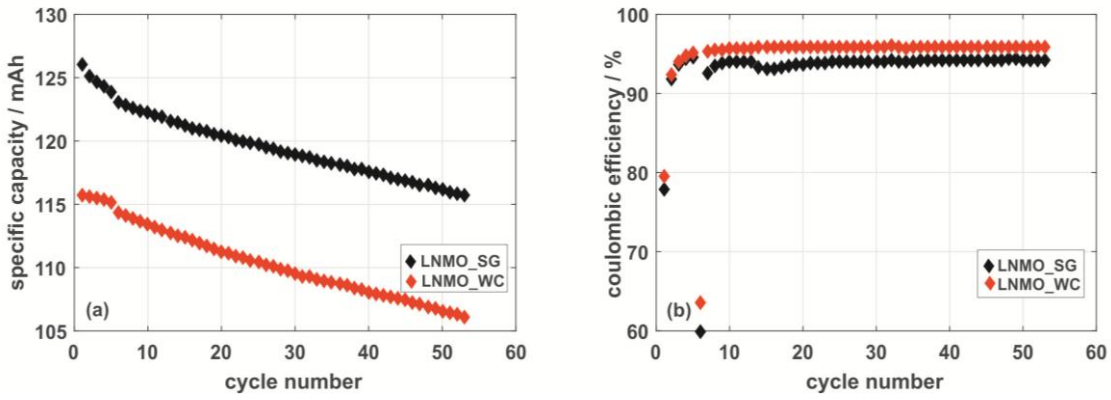

Figure 15: Cycling test performed at C/2 with EC: DMC (1:1) 1 M $LiPF_6$ electrolyte. The black dots refer to LNMO_SG and the red dots to LNMO_WC.

In Table 1, the voltage loss during self-discharge and capacities before (value of last charge capacity before OCV period) and after resting times (first value of charge capacity after OCV period) are listed. For a good cell performance a minimum in voltage loss during an OCV period is desirable. Thus, self-discharge experiments were performed. All cells provide a higher capacity before (about 120 mAh/g) resting time than after (about 118 mAh/g). The self-discharge did not differ for both materials; in both cases the potential dropped about 0.3 V. Reducing the C-rates did not significantly improve the capacities. Further experiments were therefore performed at less time consuming C/2 rates.

Table 1: Self-discharge and capacities of LNMO cathode half cells with C/2 and C/10.

C-rate	name	self-discharge / Δ V	cap. b. r. / mAh/g	cap. a. r. / mAh/g
C/2	SG 4	0.286	113	84.5
	SG 5	0.291	131	123
	WC 6	0.281	121	109
	WC 3	0.316	117	95.7
C/10	SG 19	0.282	135	0.17
	SG 16	0.911	0.56	
	WC 2	0.272	119	

2.2.2 Olivine $LiCoPO_4$ cathode material

The group of S. Brutti et al prepared $LiCoPO_4$ cathode material via a solvo-thermal method.[91] Before using the material with several additives, the material was further tested with the base electrolyte.

To investigate the oxidative behavior of LCP a CV was taken. It is shown in Figure 16. Since LCP charges and discharges over a two-phase reaction, two oxidation peaks are expected. They are visible at 4.8 V vs. Li/Li^+ and at 4.9 V vs. Li/Li^+, respectively. At 4.8 V vs. Li/Li^+ the delithination to the intermediate phase $Li_{0.6}CoPO_4$ occurs and at 4.9 V vs. Li/Li^+ it is further transformed to $CoPO_4$.

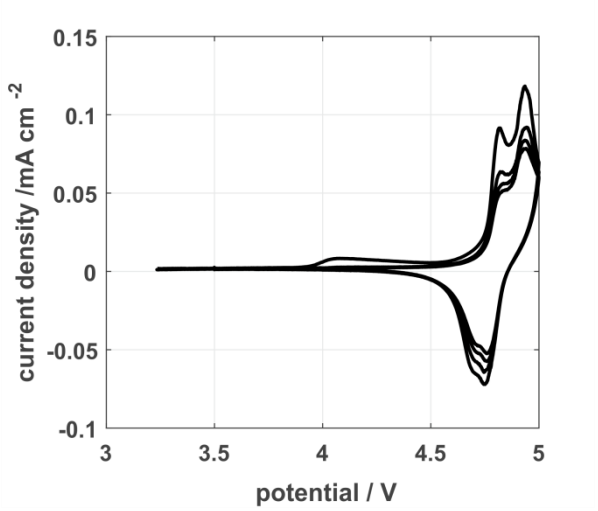

Figure 16: Cyclic voltammogram of LCP measured at 0.05 mV/s with EC:DMC (1:1) 1 M $LiPF_6$ electrolyte.

In Figure 17, the specific capacity and coulombic efficiency are plotted against the cycle number. In contrast to the spinel type LNMO cathode material, the specific capacity of the olivine type is much lower (15 mAh after 50 cycles). Additionally, the CE spreads over a wide range (43% - 56 %). This inferior cycling performance could be due to the poor electronic conductivity and instability of $CoPO_4$. [25] It tends to change fast to an amorphous state at room temperature, resulting in capacity loss.[33]

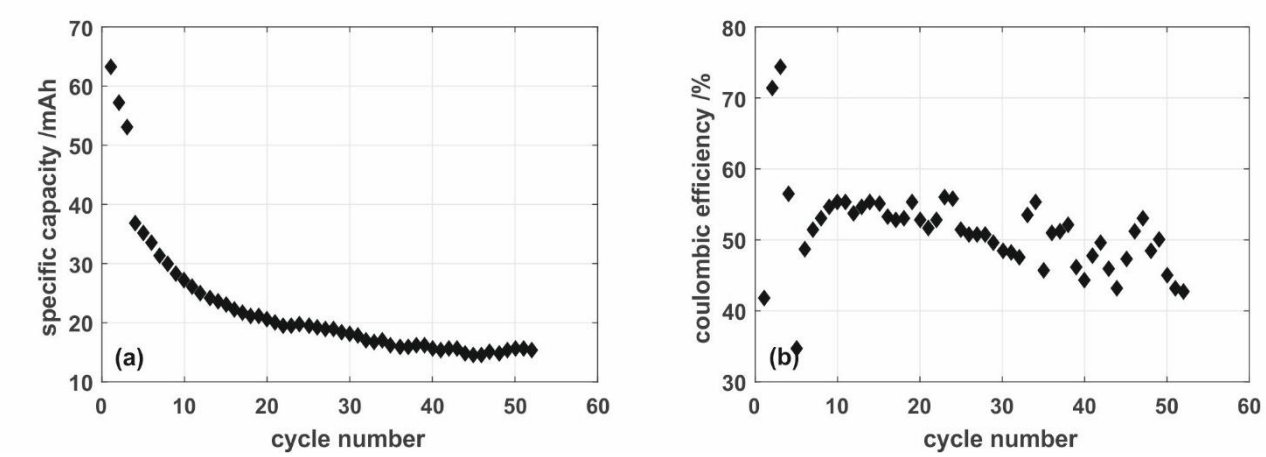

Figure 17: Galvanostatic cycling test of LCP at C/2, EC: DMC (1:1) electrolyte, 1 M $LiPF_6$, (a) specific capacity, (b) coulombic efficiency.

2.3 Surface layers on LNMO

2.3.1 *In-situ* investigations

2.3.1.1 Galvanostatic cycling tests

As shown in Figure 18, the cell with electrolyte containing SA provides the highest specific capacity (about 119 mAh) and decreases only slightly over 50 cycles. The CE lies at 96 %. The cell with electrolyte containing GA exhibits the second best performance with a specific capacity of about 99 mAh and a CE of 97 %. In contrast, the cells with an electrolyte containing silylborate or phosphate provide fluctuating CE over a wide area and the specific capacity decreases drastically. The cell containing PES as additive performs poorly showing a decrease in specific capacity and low coulombic efficiency of about 90 %, which lies below the base electrolyte (94 %).

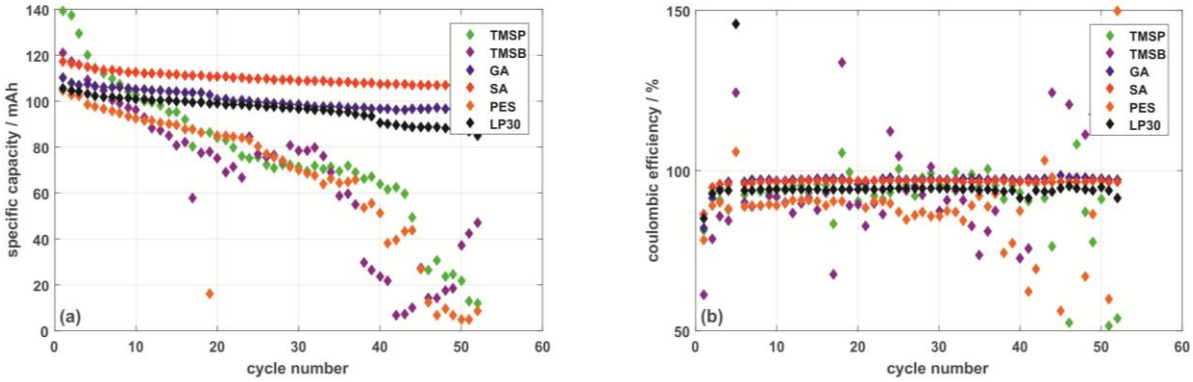

Figure 18: Specific capacity and coulombic efficiency are plotted vs. cycle number in an LP30 electrolyte with 2 wt.% additive. Test conditions: C-rate C/2, upper (5.0 V)/lower (3.5) cut-off potential.

For investigation of the self-discharge of LIBs an OCV period over 99 h was chosen. Figure 19 shows the voltage loss over time. The cell with an electrolyte containing GA provides the slightest decrease in voltage loss at the beginning. Therefore, it is a promising stabilizing agent. The cell with an electrolyte containing of SA shows also a good self-discharge performance. The cell containing of TMSP as additive exhibits only a little bit better self-discharge performance than the base electrolyte cell. Cells with electrolytes containing PES or TMSB provide no improvement. Overall, the lost capacity shows a very similar trend to the voltage decrease. The cell with an electrolyte containing GA shows the lowest capacity loss of about 34.19 mAh/g (shown in Table 2). The cell with an electrolyte containing SA exhibits a capacity loss of 52.07 mAh/g. Cells assembled with electrolyte containing TMSB or PES provide values below 74.57 mAh/g and thus provide no protection from self-discharge via a stabilizing SL.

Table 2: Capacity loss in mAh/g and percent of the measured cells, LNMO cathode.

additive	Q / mAh/g	capacity loss / %
SA	52.07	11.04
GA	34.19	7.37
PES	90.91	15.70
TMSP	60.23	9.70
TMSB	74.72	13.61
LP30	74.57	20.50

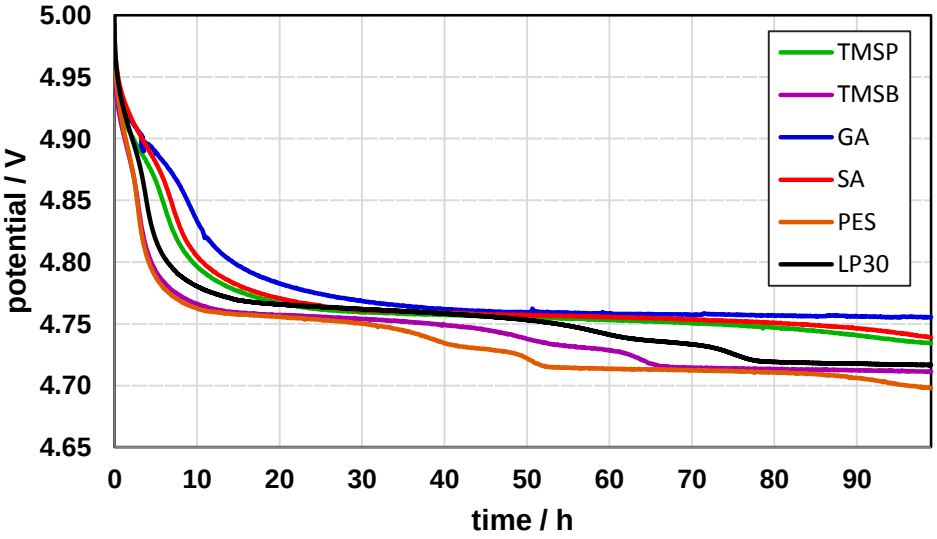

Figure 19: Self-discharge over a time range of 99 h in an LP30 electrolyte with 2 wt.% additive.

2.3.1.2 OEMS investigations

To investigate the gas evolution during cyclic voltammetry, OEMS was performed. CO_2, POF_2, C_2H_4 and H_2 are the most important and interesting gas components during the degradation of the electrolyte, which will be discussed in detail below.

The degradation of the conducting salt ($LiPF_6$) is visible in all measurements (POF_3 (m/z = 104), POF_2 (m/z = 85), POF (m/z = 66) and PO (m/z = 47)). The strongest ion flow was POF_2, which was used for further considerations. The formation mechanism of POF_3 was suggested by Tasaki et al. to concur with CO_2 evolution. [90]

$$Li_2CO_3 + LiPF_6 \rightarrow 3\ LiF + POF_3 + CO_2$$

$$Li_2CO_3 + PF_5 \rightarrow 2\ LiF + POF_3 + CO_2$$ [90]

In all measurements the formation of POF_2 correlates with the oxidation of LNMO and a peak broadening is visible, which could be due to poorly soluble, gaseous products, which are trapped as gas bubbles and thus increase the time until they are measured.[21] Moreover, Guéguen et al. investigated the $LiPF_6$ and carbonate solvent decomposition under formation of reactive species (e.g. ROH) and CO_2 when voltages greater than 4.2 V vs. Li/Li^+ are applied. Those alcohols hydrolyze the conducting salt to form POF_3.[22]

CO_2 (m/z = 44) forms if voltages greater than 4.2 V vs. Li/Li^+ are applied. In that range carbonate electrolytes and its conducting salt start to decompose under formation of CO_2 as mentioned above.

2.3.1.2.1 LP30 base electrolyte

Figure 20 shows the flux of those volatile species displaying a systematic trend during CV. The formation of POF_2 appears already at 4.6 V vs. Li/Li^+. POF_2 evolution further increases at a voltage of 4.8 V vs. Li/Li^+, which refers to the oxidation of Ni(II) to Ni(IV). A slight increase in the ion flux of ethylene and H_2 is visible, respectively. However, almost no formation of CO_2 was detected.

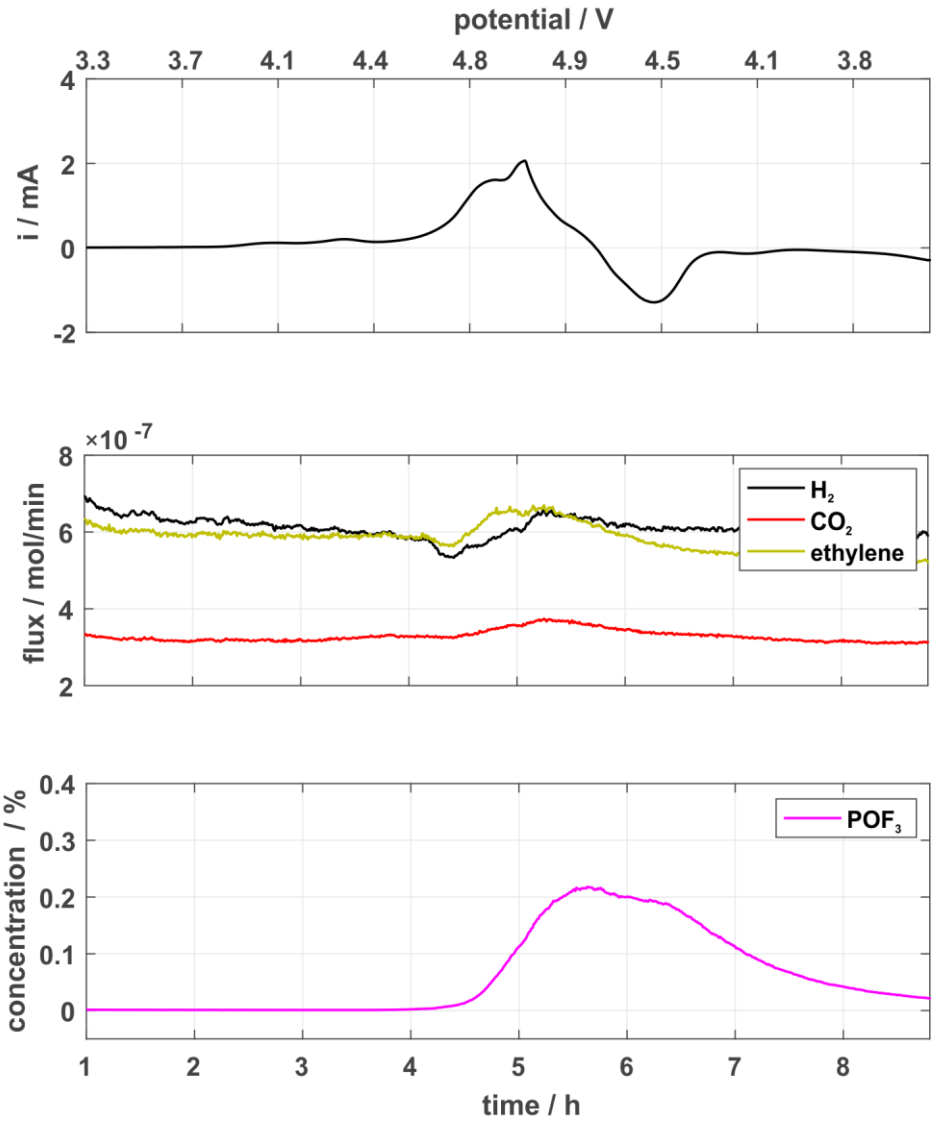

Figure 20: OEMS results with a voltage range between 3.49 - 5.00 V at a sweep range of 0.1 mV/s with purge gas of Ar. As electrolyte LP30 was used.

2.3.1.2.2 TMSB electrolyte

Figure 21 shows the OEMS results of the cell with an electrolyte containing TMSB as additive. POF_3 evolution starts at about 4.7 V with a decrease in intensity of the ion flow as in contrast to the base electrolyte. A strong evolution of ethylene and CO_2 appears at a voltage of 5.0 V vs. Li/Li^+. However, no H_2 formation was detected.

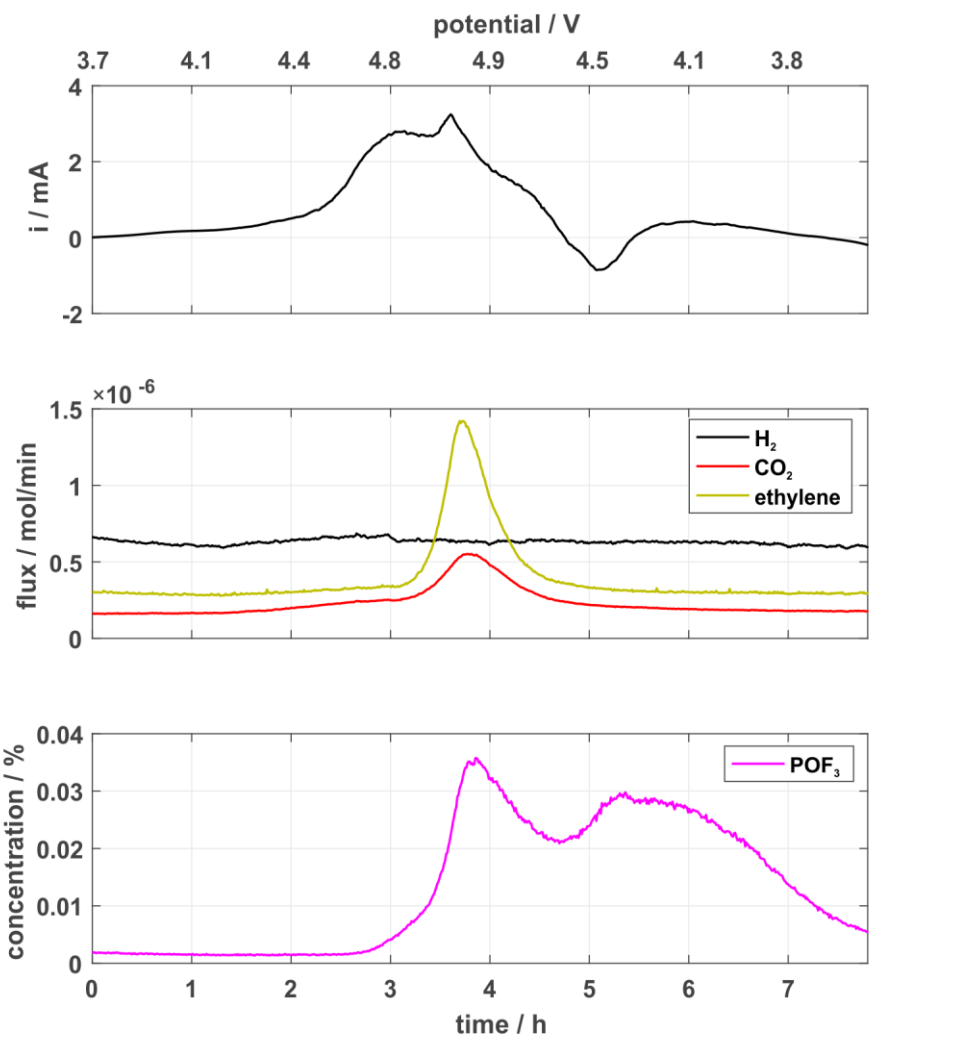

Figure 21: OEMS results with a voltage range between 3.49 - 5.00 V at a sweep range of 0.1 mV/s with purge gas of Ar. As electrolyte LP30 with 2 wt.% TMSB was used.

2.3.1.2.3 TMSP electrolyte

The OEMS cell with an electrolyte containing TMSP (Figure 22) shows a decrease in intensity of POF_2. Thus, less salt degrades. The formation of CO_2 is barely visible and the evolution of ethylene almost nonexistent. However, a formation of hydrogen at 5.0 V vs. Li/Li^+ is visible, which could be formed by additive decomposition.

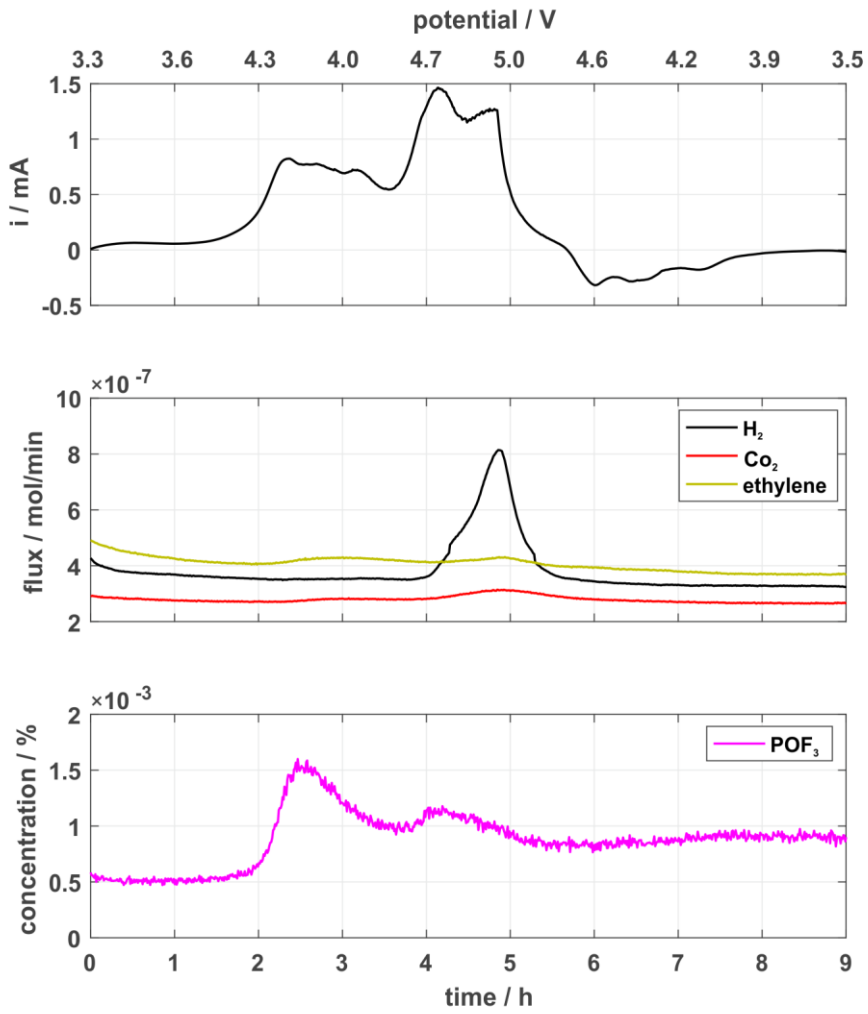

Figure 22: OEMS results with a voltage range between 3.49 - 5.00 V at a sweep range of 0.1 mV/s with purge gas of Ar. As electrolyte LP30 with 2 wt.% TMSP was used.

2.3.1.2.4 GA electrolyte

Figure 23 shows the volatile gases of an OEMS cell formed by degradation of LP30 with 2 wt.% GA. It exhibits the smallest evolution of POF_3 and thus the lowest salt degradation. Additionally, a formation of ethylene, as well as CO_2 and H_2 is visible at about 5 V vs. Li/Li^+.

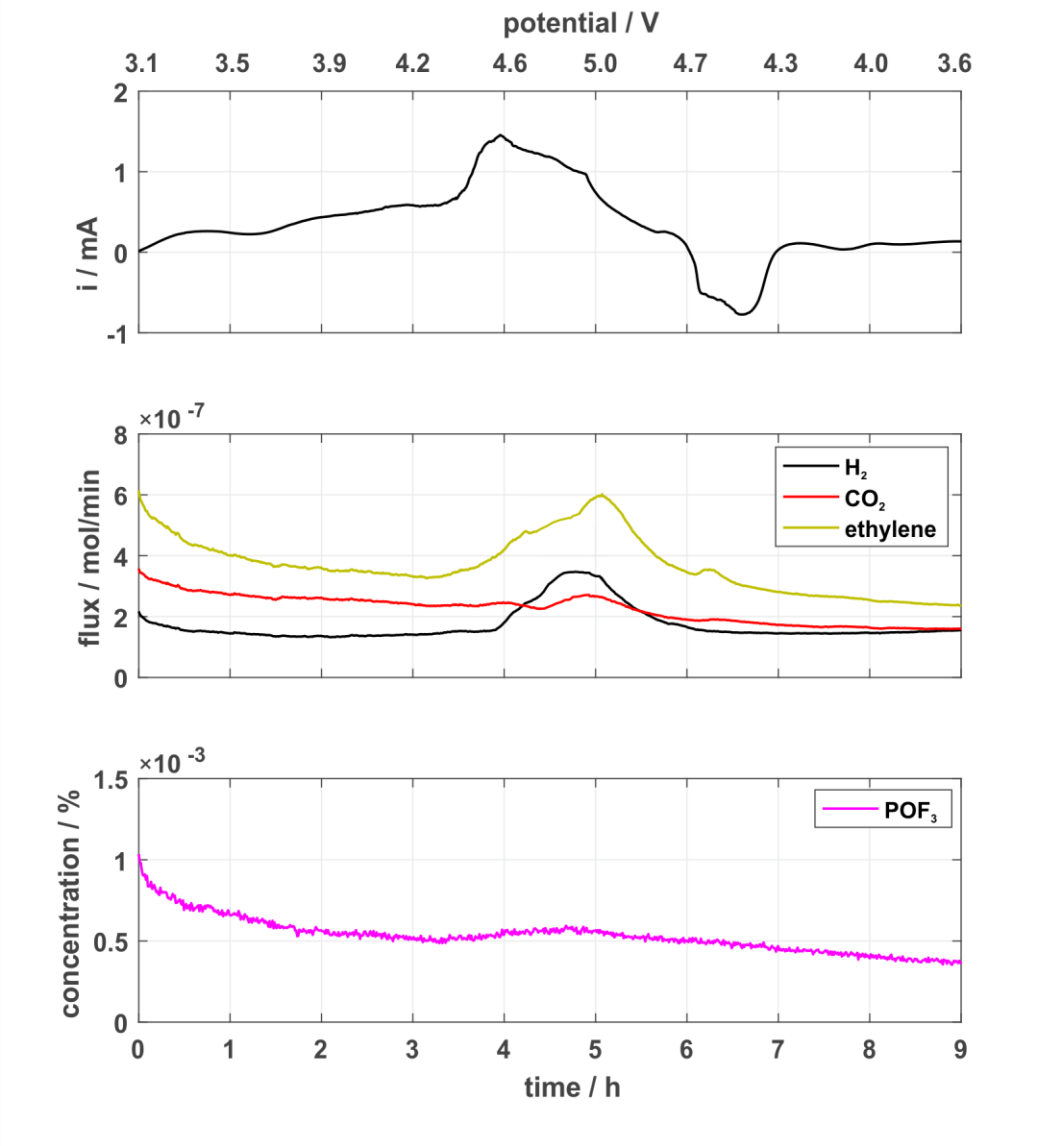

Figure 23: OEMS results with a voltage range between 3.49 - 5.00 V at a sweep range of 0.1 mV/s with purge gas of Ar. As electrolyte LP30 with 2 wt.% GA was used.

Overall, the OEMS cell containing an electrolyte with additive exhibits a lower POF_3 evolution and thus less salt degradation. The cell with GA as additive produces the lowest amount of POF_3. This matches with the results of the self-discharge test. However, no trends in H_2, CO_2 and ethylene formation can be assumed.

2.3.2 *Ex-situ* investigations

2.3.2.1 Electrochemical Impedance Spectroscopy (EIS)

In a Nyquist Plot the imaginary part is plotted against the real part. Almost all spectra consist of a depressed semicircle in the high to medium frequency range and a sloping line in the

low frequency range. The cause of the sloping line is Li^+ diffusion in the LNMO cathode.[92] The more interesting part is the depressed semicircle, that represents the interface impedance, which includes the lithium ion migration resistance R_s and charge transfer resistance R_{ct}.[93] Due to the interface impedance, a conclusion about the conductance of the formed surface layers (SL and SEI) can be made.

Figure 24 shows the Nyquist Plots of the measured impedance spectra. For all cells with an electrolyte containing additives the interface impedance of the cells measured after the 1st cycle is much smaller than for those measured after the 50th cycle. The cell with an electrolyte containing TMSP provides the smallest impedance after the first cycle, followed by the cell with the electrolyte containing SA and the cell with the electrolyte containing TMSB. The cells with electrolyte containing GA or PES exhibit the largest impedance. After 50 cycles, LP30 shows the lowest resistance. The decrease in impedance from the 50th to the 1st cycle could be due to an instable SL and SEI, which is formed upon cycling. The anhydrides display the smallest impedance after 50 cycles. PES exhibits the largest impedance.

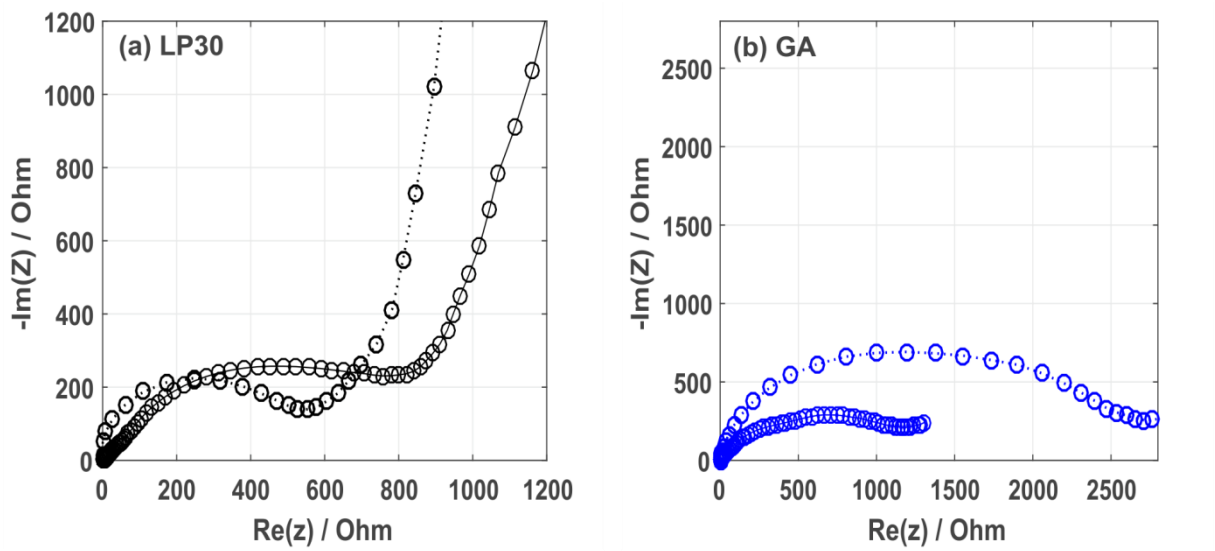

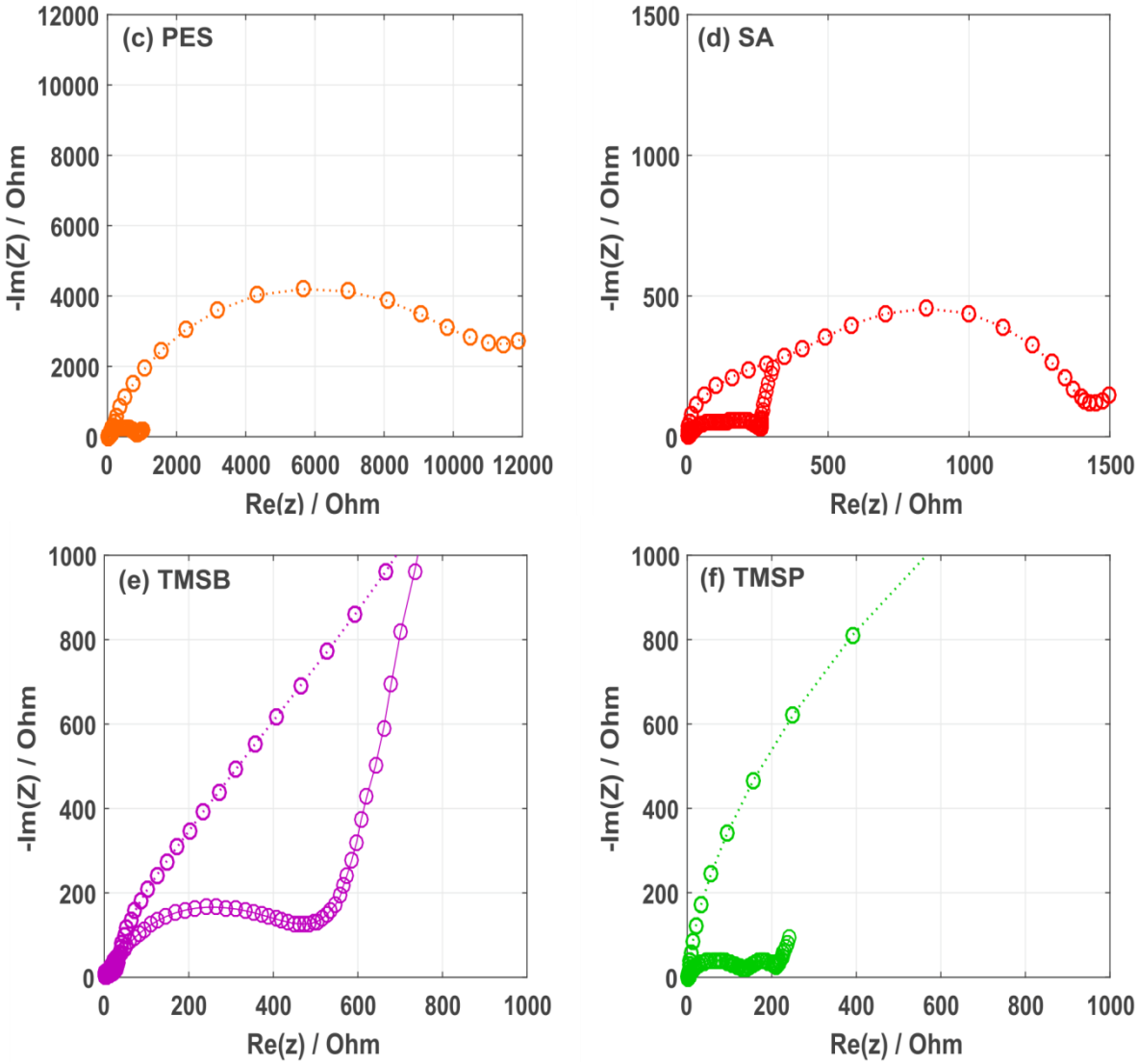

Figure 24: EIS of LNMO half-cells with LP30 electrolyte after the 1st (line) and 50th (dotted line) discharge cycle with different electrolyte additives.

2.3.2.2 NMR investigations of LNMO cathodes

^{1}H NMR in D_2O and $CDCl_3$ were taken of LNMO cathodes and separators after 50 cycles.

2.3.2.2.1 Compounds soluble in $CDCl_3$

Almost all spectra show now significant peaks for electrolyte degradation. The sample with the electrolyte containing SA is an exception that shows a signal at 3.0 ppm (singlet) as shown in Figure 25. This line could originate in the polymerization product of the additive. The COSY 2D-spectrum shows no ^{1}H coupling with the aforementioned shift, indicating a degradation product of the additive.

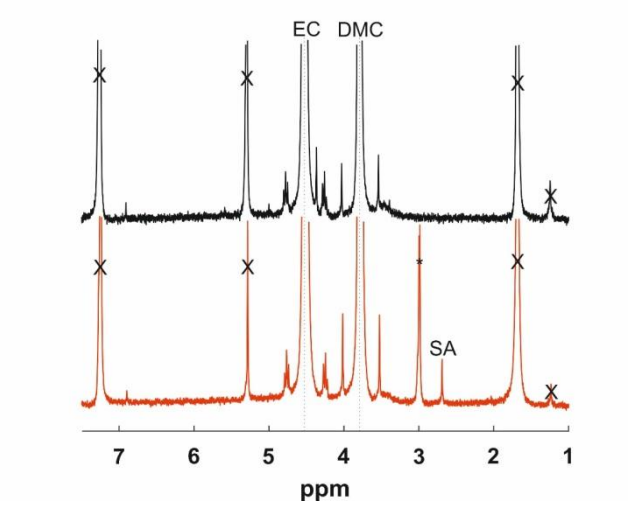

Figure 25: ^{1}H NMR taken in $CDCl_3$ of LP30 (black) and with additive SA (red) and degradation product of the additive (*).

The signals of the electrolyte are visible in all spectra at 4.5 ppm (EC) and 3.8 ppm (DMC), respectively. Impurities of grease are visible in some spectra from 1.22 to 1.25 ppm. Furthermore, an impurity of DCM (dichloromethane) is visible at 5.3 ppm. Water signals in the range of 1.6 ppm to 1.7 ppm. The peaks of all additives are listed in Table 3.

Table 3: NMR-signals of the additives and corresponding assignment.

Additive	shift / ppm	assignment	shift / ppm	assignment
SA	2.6 (s)	C-C**H$_2$**- C**H$_2$**-C		
GA	2.4 (t)	C-C**H$_2$**-CH$_2$	2.0 (qi)	CH$_2$-C**H$_2$**-CH$_2$
PES	6.9 (m)	CH$_2$-C**H**- C**H**-S	5.1 (t)	O-C**H$_2$**-CH
TMSB	1.6 (s)	C**H$_3$**-Si		
TMSP	1.6 (s)	C**H$_3$**-Si		

2.3.2.2.2 Compounds soluble in D_2O

To better characterize the SL, a ^{1}H NMR was taken with D_2O as a solvent. The decomposed electrolyte products produce the main peaks. Figure 26 shows the NMR spectra.

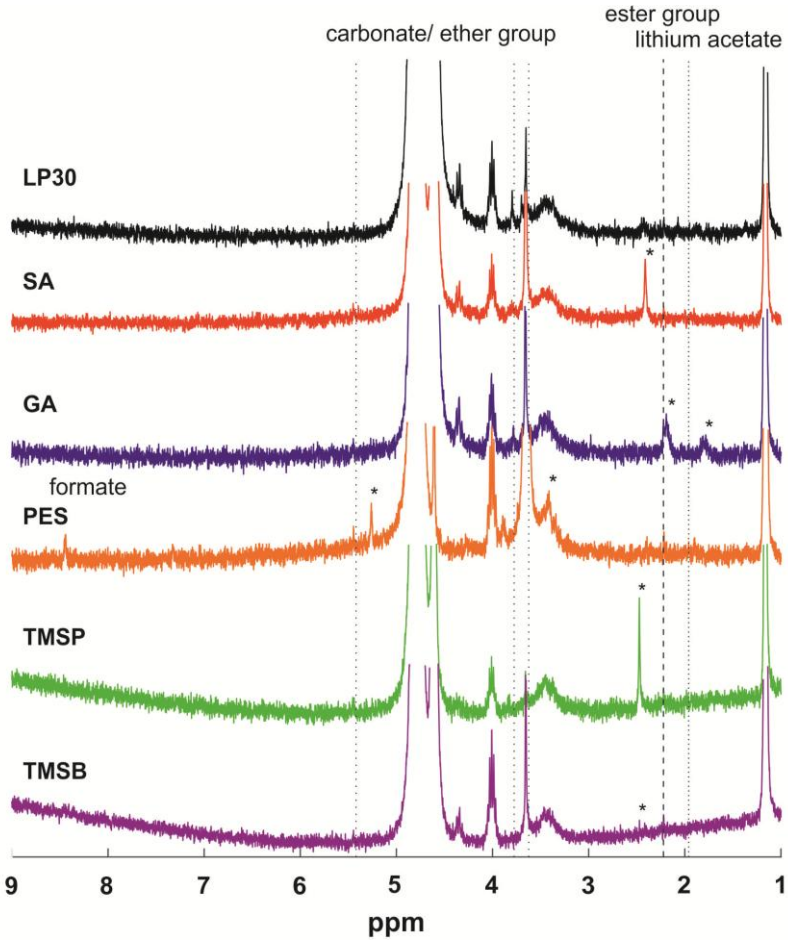

Figure 26: ^{1}H-NMR spectra taken in D_2O with degradation products of the additives marked (*), carbonate/ether group (. . .) and ester group (- - -).

Peaks, which are visible in all spectra, correspond to the degradation products of the electrolyte, especially of EC. Mostly, a polymerization reaction occurs. A possible mechanism was suggested by Yang et al. (see following scheme).[73]

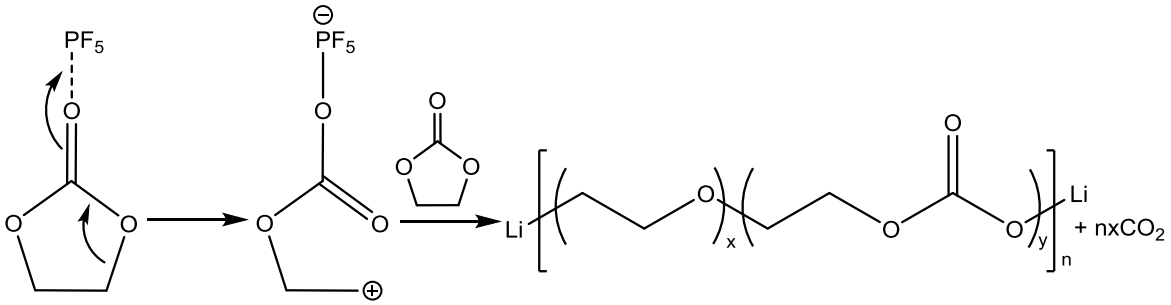

Scheme 1: Degradation of ethylene carbonate.

PF_5 serves as a catalyst to oxidize EC on the delithated LNMO surface at charging potentials higher than 4.3 V.[72,73] The ether species exhibit signals at 5.45 ppm, 3.7 ppm and 3.65 ppm. Other organic compounds like C=O or carbonate compounds (CO_3)[94] appear in the range

between 3.8 ppm – 3.6 ppm. As they are present in almost all spectra, they likely originate from the electrolyte solvent and could also contribute to the SL. The signal at 2.2 ppm could correspond to an ester group, which could be formed by the degradation of the electrolyte. This line is visible in almost all spectra. Lithium acetate displays at a signal of 1.9 ppm, but is only visible in samples with electrolytes containing PES, SA or GA.

An impurity of the binder appears at 1.16 ppm, which corresponds to polyvinylidenfluoride (PVDF). Further impurities were produced through EC and DMC, which were not completely washed away. All samples contain degradation products. Their signals are listed in Table 4.

Table 4: Degradation signals of the additives on LNMO cathode.

Additive	shift / ppm	assignment	shift / ppm	assignment
SA	2.4 (s)	C-C**H$_2$**- C**H$_2$**-C		
GA	3.0 (s)		2.2 (t)	C-C**H$_2$**-CH$_2$
	1.8 (qi)	CH$_2$-C**H$_2$**-CH$_2$		
TMSP	2.5 (s)			
TMSB	2.5 (s)			
PES	5.26 (s)		3.34 (s)	

For the sample with an electrolyte containing GA, the signals appear in comparison to the $CDCl_3$ spectra, 0.2 ppm into the higher field. Thus, it can be assumed that a polymerization of glutaric anhydride occurred, which exhibits a similar line pattern. This polymerization could be catalyzed by water or an alcohol. Figure 27 shows the degradation mechanism of LP30 containing GA.

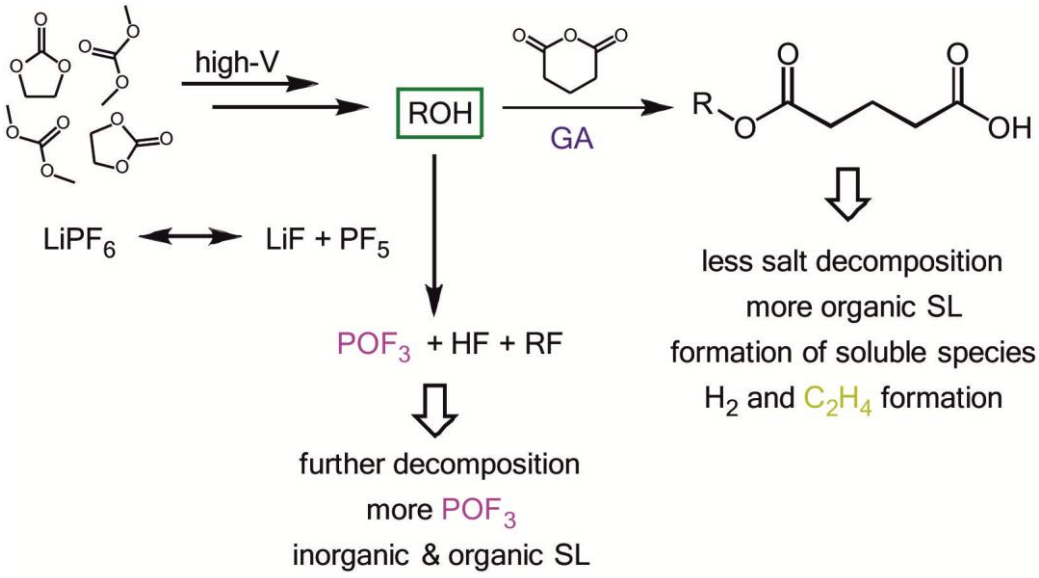

Figure 27: Degradation mechanism of LP30 with GA present.

Another possibility is the integration of GA into the SL, which leads to a highfield shift, due to a different environment.

Succinic anhydride could react similarly to GA due the similarity in molecular structure. Thus, a polymerization reactions occurs, which is catalyzed by water or alcohol.

The sample with the electrolyte containing PES exhibits NMR-signals of degradation products at 8.45 ppm, 5.26 ppm and 3.34 ppm. The line at 8.45 ppm is characteristic for methylformate. The main degradation product appears at 5.26 ppm. However, no clear mechanism or structure can be proposed based solely on this data.

The samples with the electrolyte containing silylphosphate or borate exhibit a line at 2.5 ppm, which indicates a product peak. No signals appear in the range around 0 ppm, which is characteristic for silane and siloxane groups. Thus, it can be assumed that the degradation product of the additive is not soluble in D_2O.

2.3.2.3 FTIR investigations

FTIR spectra were taken to further investigate the SL. Figure 28 shows the FTIR spectra of the different samples.

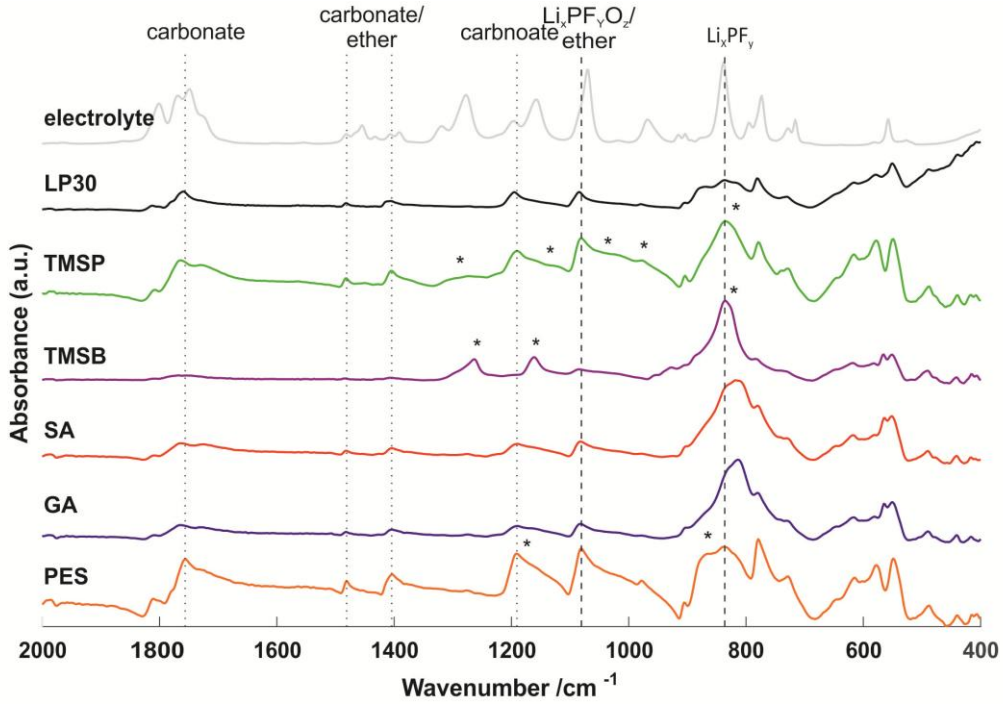

Figure 28: FTIR spectra of electrodes after five formation cycles with various additives in LP30 electrolyte. Test conditions: C-rate C/2, upper (5.0 V)/lower (3.5) cut-off potential.

Clearly, polyethylene carbonate is formed, which has significant bands at 1760 cm^{-1} and 1200 cm^{-1}. The C=O vibration of the ester group is visible at 1760 cm^{-1}. Its C-O vibration appears at about 1196 cm^{-1} and 1085 cm^{-1}, respectively. The ether C-O symmetric stretching appears at 1086 cm^{-1}. Additionally, salt degradation products are visible with characteristic bands at 1085 cm^{-1} and 836 cm^{-1}, respectively. An overview over the band assignment is given in Table 5.

Table 5: Assignment of the FTIR peaks of the LNMO cathode.

$\tilde{\nu}$ / cm^{-1}	functional group	vibration	Intensity	SA	GA	PES	TMSB	TMSP	LP30
1812-1760	C=O	assym. stretch.	m-w	X	X	X		X	X
1481	$C-H_2$	assym. siccoring	w	X	X	X		X	X
1402	O-C-OO CH_2	assym. stretch. twisting	w	X	X	X		X	X
1196	COCOO	deform.	m	X	X	X		X	X

	COC	deform.							
1085	OCO	asym.	m	X	X	X	X	X	X
	COC	stretch.							
	$Li_xPF_YO_z$	symm.							
		strech.							
836	Li_XPF_y		s	X	X	X	X	X	X
616			w	X	X	X	X	X	X
550	LiF		w	X	X	X	X	X	X

s..strong, m…medium, w…weak

Characteristic oxidation products of the additives are shown in Table 6. For the samples with electrolyte containing silyl additives their main bands appear at 1259 cm^{-1} and 977 cm^{-1}(TMSP) and at 1265 cm^{-1} and 1165 cm^{-1} and for both at 836 cm^{-1}, respectively. The siloxane moiety (Si-OR) is present in the phosphate as well as in the borate sample at about 1260 cm^{-1}. The band at 1165 cm^{-1} could not be assigned unambiguously. However, it can be assumed that this band belongs to a borate group (B-OR). A vibrational mode of the phosphate oxide group should appear in between a wavenumber of 1100 and 1200 cm^{-1}.[95] In this area a small absorption band is visible, which indicates a P = O group. At 977 cm^{-1} a P-OR group is visible. At about 820 cm^{-1} the band of the samples of TMSB and TMSP is broader, which could indicate a Si – O vibration at this position.

The sample with electrolyte containing prop-1-en sultone shows characteristic bands at 1195 cm^{-1} and 875 cm^{-1}, which belong to the sulfoxide and ester group, respectively.

Both anhydrides form a polymer consisting of carbonate groups, which are similar to the formed degradation products of the electrolyte, which is consistent with the NMR data. Thus, they exhibit no original bands that are absent in the base electrolyte. Guyomard et al. already proposed that in the presence of GA, the SL consists of a larger fraction of organic and less inorganic compounds.[16]

Table 6: Assignments for degradation products of additives on a LNMO cathode.

TMSB			TMSP		
$\tilde{\nu}$ / cm^{-1}	functional group	Intensity	$\tilde{\nu}$ / cm^{-1}	functional group	Intensity
1265	Si-CH_3	s	1259	Si-CH_3	w
1165	B-OR	s	1150	P=O	w
836	Si-O	s	1042	Si-OR	m
PES			977	P-OR	m
$\tilde{\nu}$ / cm^{-1}	functional group	Intensity	836	Si-O	s
1195	S=O	m			
875	S-OR	s			

s..strong, m…medium, w…weak

2.4 Preliminary results on $LiCoPO_4$

2.4.1 *In-situ* investigations

2.4.1.1 Galvanostatic cycling

Figure 29 presents the specific capacities and coulombic efficiencies against the cycle number of cells containing a LCP cathode and electrolyte without or with additive. Figure 29 (a) shows the specific capacities of all cells with electrolytes containing additives or no additives. All capacities are beyond the base electrolyte. The electrolyte containing TMSP provides by far the best performance. It grants a specific capacity of 23 mAh after 50 cycles and a coulombic efficiency of 97 %, which exceeds all other tested additives. The second best performance exhibits the cell with the electrolyte containing GA with a specific capacity of 21 mAh and coulombic efficiency of 88 %. Only the cells with electrolytes containing TMSP or GA grant better coulombic efficiencies than the base electrolyte (80 %). The cells with electrolytes containing SA or PES slightly outperform the cell with the base electrolyte with coulombic efficiencies of 75 % and 72 %, respectively. The cell with the electrolyte containing TMBS provides an inferior performance, because after self-discharge testing no reversible cell performance occurs. Thus, it is not shown in the figure below.

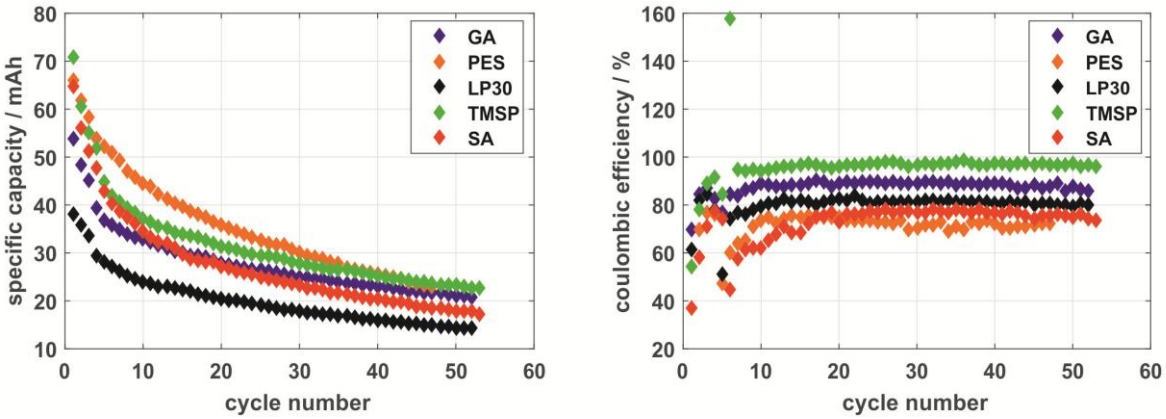

Figure 29: Specific capacity and coulombic efficiency are plotted vs. cycle number in a LP30 electrolyte with 2 wt.% additives and a LCP cathode. Test conditions: C-rate C/2, upper (5.0 V)/lower (3.5) cut-off potential.

The overall bad cell performance is a result of an instable $CoPO_4$ phase and an uncoated cathode material. Brutti et al. investigated uncoated LCP materials. They provide a specific capacity of about 50 mAh/g (at C/2). At a C-rate of C/10 the specific capacity reached about 100 mAh/g after 10 cycle.[96]

Again, the self-discharge was investigated through an OCV period over 99 h. Figure 30 shows the voltage loss over time. Capacity loss values are listed in Table 7. The cell with the electrolyte containing TMSP provides a good cell performance, which is consistent with improved capacity retention as compared to the cell with the base electrolyte. It suppresses self-discharge almost completely with a capacity loss of only 9.98 %. It is followed by the cell with an electrolyte containing GA with a loss of 25.35 %. All cells with the electrolyte containing additives provide a positive influence as determined by capacity loss, since their values lay above the cell with the base electrolyte (32.19 %). However, the cell with the electrolyte containing TMSB exhibits a great voltage loss (almost 2 V). Thus, it provides the worst self-discharge performance.

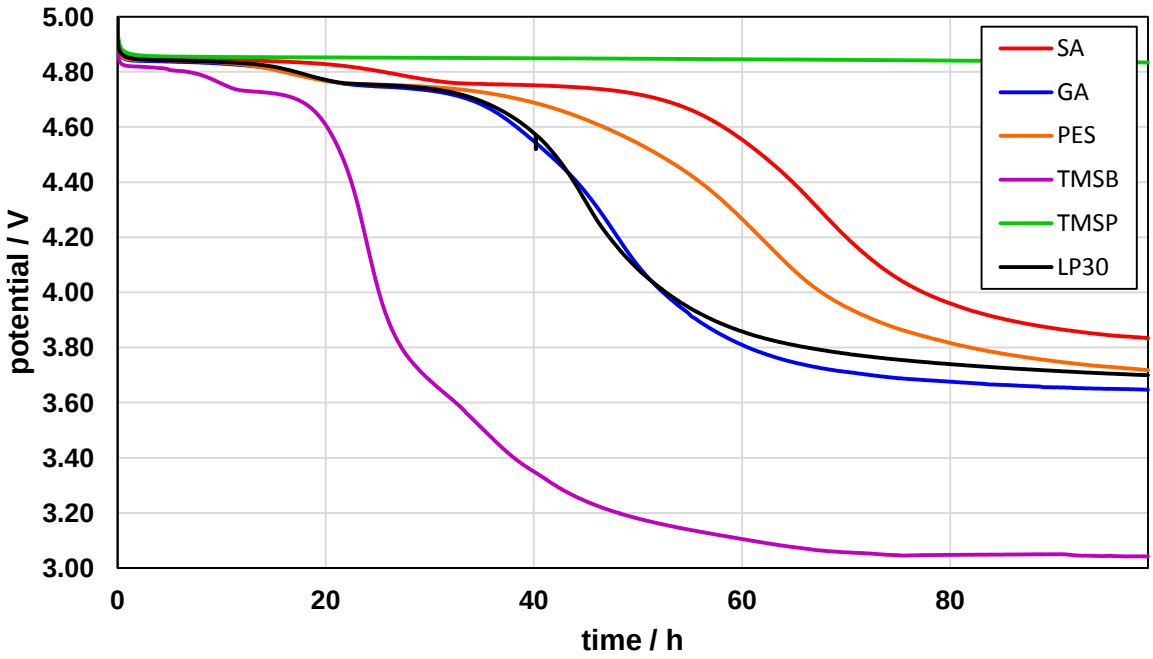

Figure 30: Self-discharge of cells with a LCP cathode are tested over a time range of 99 h in a LP30 electrolyte with 2 wt.% additive.

Table 7: Capacity loss in mAh/g and percent of the measured cells with an LCP cathode.

additive	Q/ mAh/g	capacity loss/ %
SA	96.47	31.4
GA	66.58	25.35
PES	101.44	30.96
TMSP	25.08	9.98
TMSB	79.73	20.24
LP30	109.34	32.19

2.4.2 *Ex-situ* investigations

2.4.2.1 Electrochemical Impedance Spectroscopy (EIS)

The impedance spectra of cells with LCP cathode materials and different additives are shown in Figure 31. The interphacial impedance, which represents the SL and SEI, is after the first cycle in all cells smaller than after cycling fifty times. The cell with the electrolyte containing TMSP provides the smallest impedance after the 1st and 50th cycle, which is consistent with high cyclability, CE and low self-discharge. The cells with electrolytes containing anhydrides exhibit the second best performance after the 1st cycle. However, after the 50th cycle all cells with electrolyte containing additives, except TMSP provide a drastic

increase in interface impedance, which is reflected by their low CE and cycling performances.

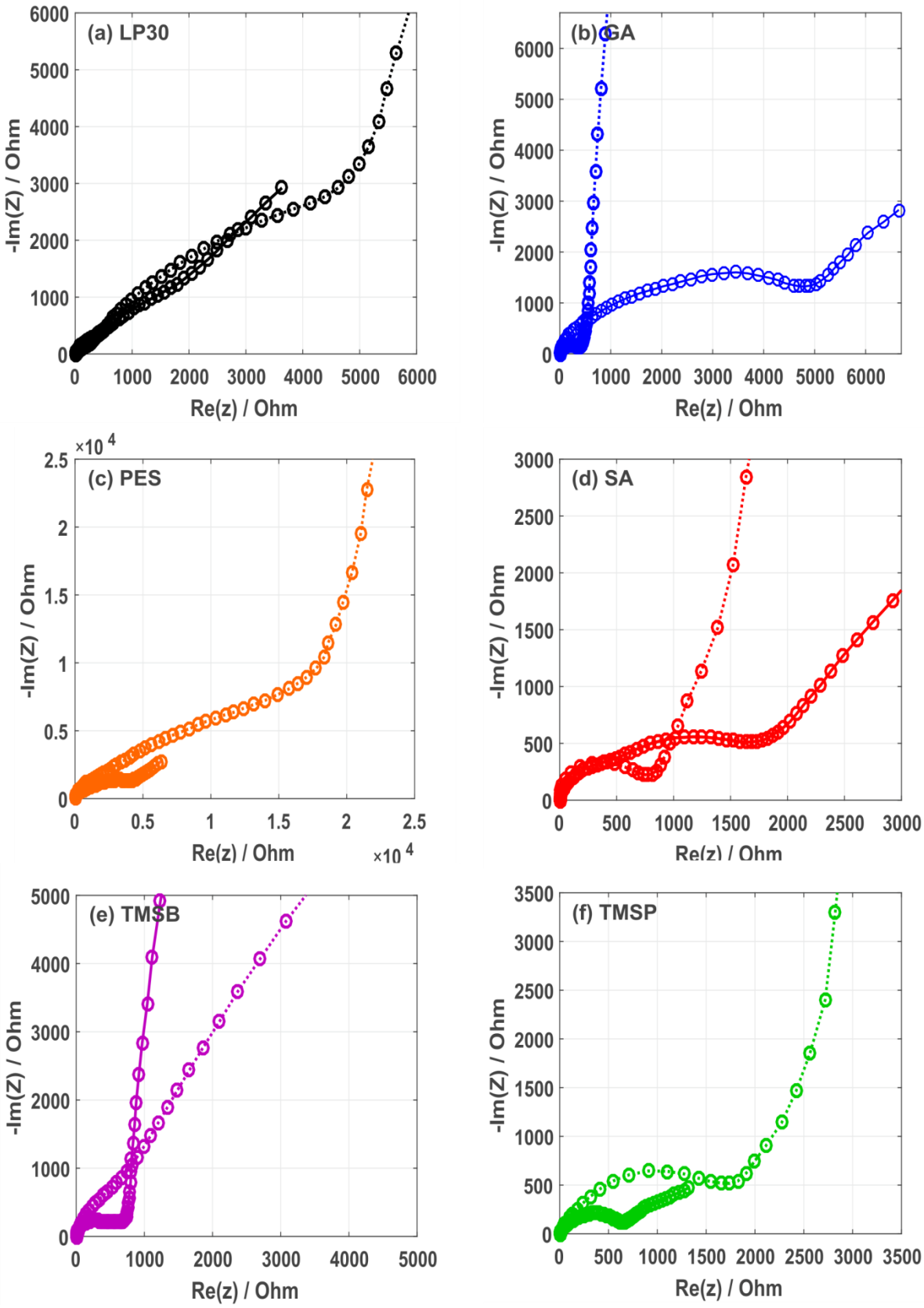

Figure 31: EIS of LCP half-cells with LP30 electrolyte after the 1st (line) and 50th (dotted line) charge/ discharge cycle with different electrolyte additives.

2.4.2.2 NMR investigations of LNMO cathodes

Investigation of the compounds composing the surface layer was done via ^{1}H NMR. Therefore, degradation products soluble in $CDCl_3$ and D_2O were analyzed.

2.4.2.2.1 Compounds soluble in $CDCl_3$

The NMR spectra of LCP show almost the same signal pattern than in LNMO NMR spectra. The main lines appear at 4.5 ppm and 3.8 ppm. They can be assigned to the electrolyte, whereas signals of EC appear at lower and those of DMC at higher field. The additives show no degradation products, with an exception of SA and PES. The degradation product of SA appears at 3.0 ppm, similar to the case of the LNMO cathode. For the sample with the electrolyte containing PES two singlets appear at 3.6 ppm and 3.4 ppm. Figure 32 shows the NMR spectra of samples with the electrolyte containing LP30, SA or PES.

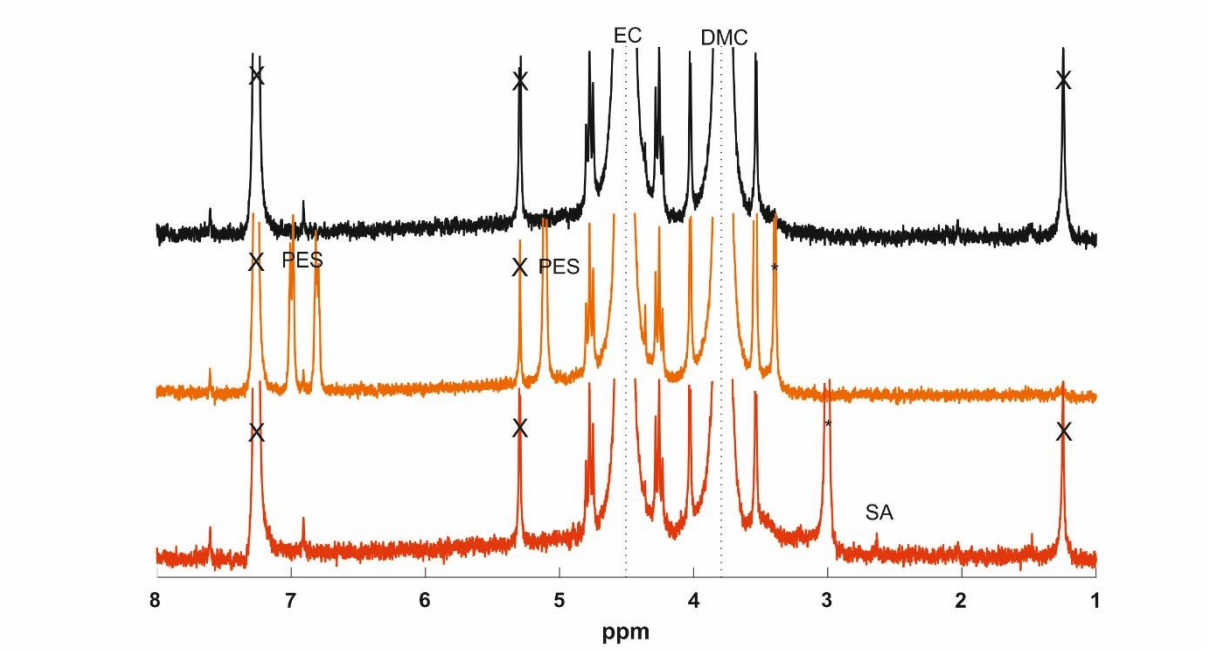

Figure 32: ^{1}H NMR taken in $CDCl_3$ of LP30 (black), with additive PES (orange) and SA (red) and degradation product of the additives (*).

Grease was found in a few samples at 1.25 ppm. Another impurity appears at 5.3 ppm, which belongs to dichloromethane. The shifts corresponding to the non-degraded additives are listed in Table 8. Both additives consisting of silylgroups show a line at 0.2 ppm, which corresponds to the trimethylsilylgroup. SA displays a small singlet at 2.6 ppm. At 2.7 ppm and 2.0 ppm the additive signals of GA are visible. For the sample with the electrolyte containing PES lines appear at 6.9 ppm and 5.1 ppm.

Table 8: NMR-signals of the decompose products on $LiCOPO_4$ and corresponding assignment.

Additive	shift / ppm	assignment	shift / ppm	assignment
SA	2.6 (s)	C-C**H$_2$**- C**H$_2$**-C		
GA	2.7 (t)	C-C**H$_2$**-CH$_2$	2.0 (qi)	CH$_2$-C**H$_2$**-CH$_2$
PES	6.9 (m)	CH$_2$-C**H**- C**H**-S	5.1 (t)	O-C**H$_2$**-CH
TMSB	0.2 (s)	C**H$_3$**-Si		
TMSP	0.2 (s)	C**H$_3$**-Si		

2.4.2.2.2 Compounds soluble in D_2O

Figure 33 shows the degradation products soluble in D_2O.

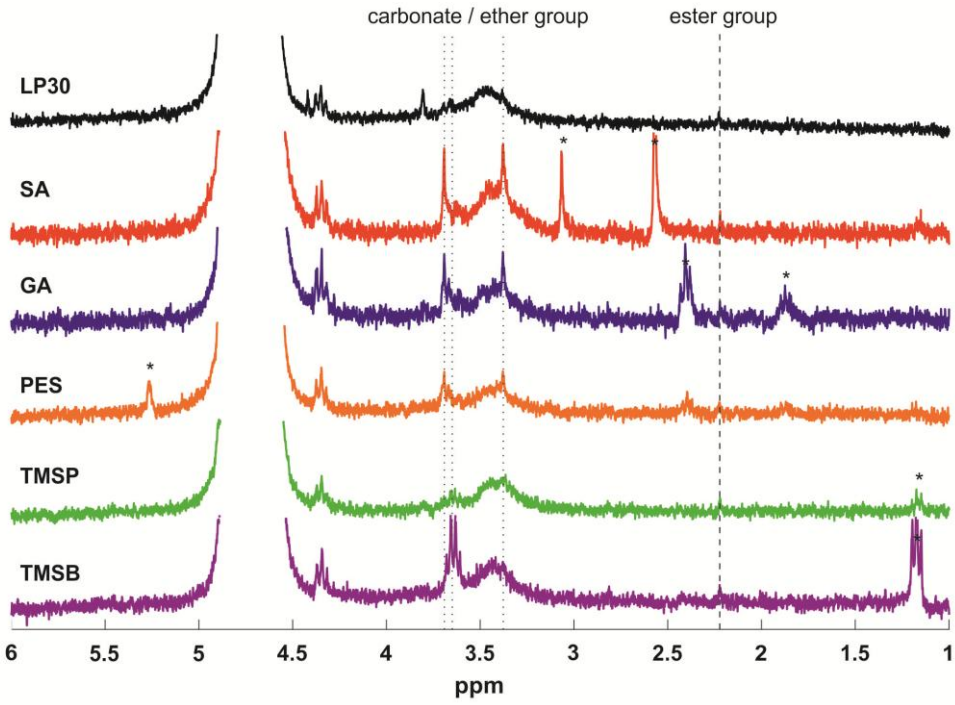

Figure 33: ^{1}H-NMR spectra taken in D_2O with degradation products of the additives (*), carbonate/ether group (. . .) and ester group (- - -). Test conditions: C-rate C/2, upper (5.0 V)/lower (3.5) cut-off potential.

The electrolyte degrades as proposed in Scheme 1. Thus, EC forms a polymer consisting of carbonate and ether groups. In the range between 3.62 ppm to 3.69 ppm these degradation

products are visible in the spectra. An ester functional group appears at 2.22 ppm in all spectra.

The degradation products of the additives on LCP appear almost at the same lines than on the LNMO cathode indicating similar soluble reaction products. The signals are listed in Table 9.

Table 9: NMR-signals of the decompose products on $LiCOPO_4$ and corresponding assignment taken in D_2O

Additive	shift / ppm	assignment	shift / ppm	assignment
SA	3.1 (s)	C-C**H$_2$**- C**H$_2$**-C	2.57 (s)	
GA	2.4 (t)	C-C**H$_2$**-CH_2	1.8 (qi)	CH_2-C**H$_2$**-CH_2
TMSP	3.65 (q)	CH_3-C**H$_2$**-CH	2.8 (s)	CH_3-CH_2-C**H**
	1.2 (t)	C**H$_3$**-CH_2-CH		
TMSB	3.65 (q)	CH_3-C**H$_2$**-CH	2.8 (s)	CH_3-CH_2-C**H**
	1.2 (t)	C**H$_3$**-CH_2-CH		
PES	5.26 (s)			

Cells assembled with the electrolyte containing succinic or glutaric anhydride contained similar polymerization products than proposed for the LNMO surface, as indicated by almost identical peak shifts. Both anhydrides degrade by forming a polymer, which is catalyzed by water or an alcohol.

PES displays a signal at 5.26 ppm which corresponds to the additive degradation product. Due to same signal patterns observed for the LCP and the LNMO cathode, the same degradation product can be assumed.

For the samples with the electrolyte containing silyl-additives ethanol has been formed. Corresponding lines appear at 3.65 ppm, 2.8 ppm and 1.2 ppm, respectively.

2.4.2.3 FTIR investigation

For the samples with LCP cathodes the bands appear almost at the same position as on LNMO cathodes. This further supports the conclusion that the overall electrolyte reduction is similar regardless of the electrode material. The FTIR spectra are shown in Figure 34.

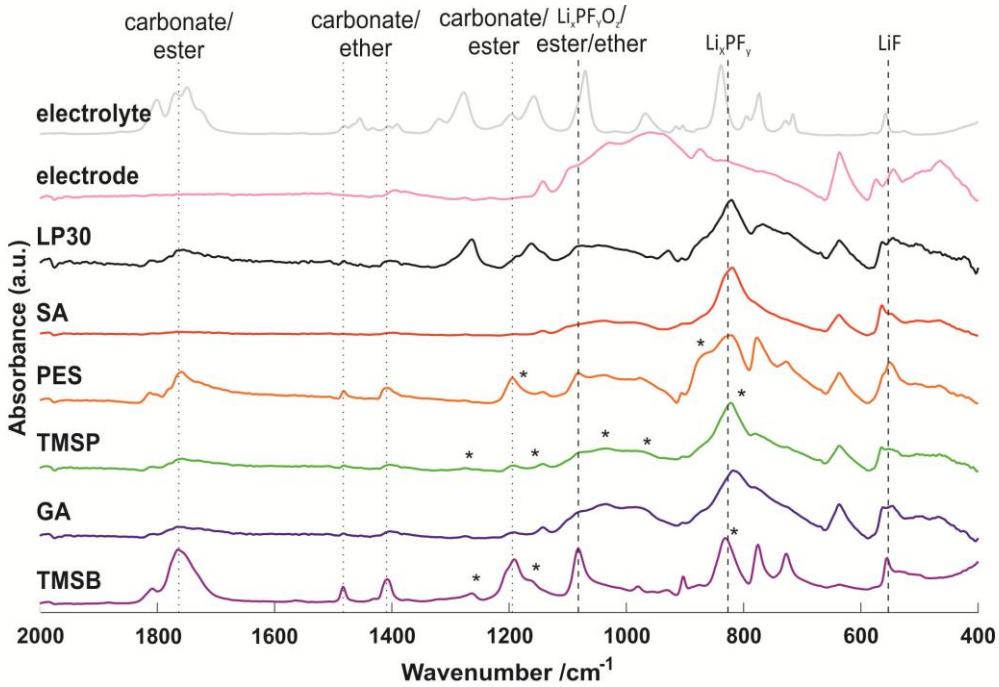

Figure 34: FTIR of LCP electrodes after five formation cycles. Test conditions: C-rate C/2, upper (5.0 V)/lower (3.5) cut-off potential.

Table 10 shows bands with the corresponding assignments. The C=O stretching vibration of a carbonate or ester group appear in the range between 1805 – 1718 cm^{-1} with different intensities. The vibration at 1196 cm^{-1} is characteristic for a carbonate or ester C-O-C deformation. The salt degradation is visible at 1085 cm^{-1} ($Li_xPF_YO_z$) and 836 cm^{-1} (Li_XPF_y). The vibration at 555 cm^{-1} is characteristic for LiF and is found on all electrode surfaces. The cathode material shows characteristic bands at 1140 cm^{-1} (P=O) and at 1085 – 963 cm^{-1} (P-O-R).

Table 10: Assignment for FTIR bands of the decompose products on $LiCOPO_4$.

$\tilde{\nu}$ / cm^{-1}	functional group	vibration	Intensity
1805-1718	C=O	assym. Stretch.	m-w
1485	$C-H_2$	assym. Siccoring	w
1406	O-C-OO	assym. stretch.	w
	CH_2	twisting	
1196	COCOO	deform.	m
	COC	deform.	
1140	P=O		
1085-963	OCO	asym. stretch.	m
	COC	symm. strech.	
	$Li_xPF_YO_z$		

	POR		
836	Li_XPF_y		s
638			w
555	LiF		w

s..strong, m…medium, w…weak

The samples with the electrolytes containing anhydrides show no significant bands differing from the base electrolyte. This could be due to the formation of similar degradation products. In both cases esters are formed. The sample with the electrolyte containing PES shows characteristic bands at 1196 cm^{-1} and 873 cm^{-1}, reflecting the S=O and the S-O-R functional groups, respectively. The sample with the electrolyte containing TMSB exhibits frequency bands at 1265 cm^{-1}, 1161 cm^{-1}, 1084 cm^{-1} and 830 cm^{-1}. The band at 1161 cm^{-1} could correspond to a boron-ester group. The other bands refer to silane and siloxane groups. The cathode surface with the electrolyte containing tris(trimethylsilyl)phosphate as additive displays silane and siloxane bands at 1275 cm^{-1}, 1080 cm^{-1} and 830 cm^{-1}, respectively. The phosphate bands appear at 1142 cm^{-1} and 1084 – 963 cm^{-1}. However, a definitive band assignment remained challenging due to the broad peak of the LCP material.

v

Table 11: Assignments for degradation products of additives on $LiCOPO_4$.

TMSB			**TMSP**		
$\tilde{\nu}$ / cm^{-1}	**functional group**	**Intensity**	**$\tilde{\nu}$ / cm^{-1}**	**functional group**	**Intensity**
1265	Si-CH_3	w	1275	Si-CH_3	w
1161	B-OR	w	1142	P=O	w
1084	Si-OR	w	1080	Si-OR	m
830	Si-O	s	1084-963	P-OR	s
PES			830	Si-O	s
$\tilde{\nu}$ / cm^{-1}	**functional group**	**Intensity**			
1196	S=O	m			
873	S-OR	s			

s..strong, m…medium, w…weak

3 Conclusion and Outlook

3.1 LNMO spinel cathode material

In this work the surface layer on the LNMO cathode as well as the electrochemical performance of half-cells was characterized with and without TMSB, TMSP, PES, SA and GA additives. The cells with the electrolyte containing anhydrides SA or GA showed the best cycle performance in galvanostatic cycling. The cell with the electrolyte containing succinic anhydride exhibited a CE of 96 % and a specific capacity of 119 mAh after 50 cycles. The cell with the electrolyte containing GA reached a specific capacity of 99 mAh and a CE of 97 %. All the other cells with electrolyte containing additives reached lower performances than the cell with the base electrolyte (specific capacity 88 mAh; CE 94 % after 50 cycles). The cell with the electrolyte containing GA most effectively suppressed self-discharge with a capacity loss of 7.37 % over the period of 99 h. The cell with the base electrolyte showed the worst performance and lost 20.50 % of its capacity.

EIS measurements of the cycled cells (after 1 and 50 cycles) provided information about the evolution of resistance of the SL and SEI. After one cycle, cells containing TMSP exhibited the smallest impedance, followed by the cells containing SA and TMSB, respectively. After 50 cycles the cell with LP30 provided the smallest impedance. The cells containing SA or GA exhibited the largest conductivity.

The SL formation was characterized via *in-situ* OEMS and *ex-situ* NMR and FTIR. The base electrolyte resulted in a surface layer consisting of organic polymers with carbonate, ether and ester functional groups and lithium salts (Li_xPF_y, $Li_xPF_yO_z$). The degradation products of the base electrolyte were also observed in the samples containing additives. The samples containing anhydrides exhibited organic compounds similar to the degradation products of the base electrolyte. The cells containing GA further suppresses salt degradation as confirmed via OEMS. The silyladditives showed the formation of siloxanes and oxides in the SL and also inhibited salt degradation. The SL of PES containing electrolyte consisted of sulfoxides and ester groups. Overall, the anhydrides showed the best performance, improved cycling stability and coulombic efficiency whilst almost completely inhibiting salt decomposition.

Future work should concentrate on further OEMS investigations, since only full cells were characterized. This presents a critical gap in the scientific literature and will yield well noticed publications. The review of so far published work on OEMS highlights furthermore the difficulty in setting up top-notch OEMS setups. In this respect the here available setup

appears clearly superior over the setups described at other labs in terms of sensitivity, quantification, and versatility. Moreover, OEMS investigations combined with galvanostatic cycling should be assembled to gain better understanding of the degradation mechanism. The SL should be further characterized, on whether organic or inorganic compounds have been formed.

3.2 LCP cathode material

This work provides characterization of SL on LCP cathode. Electrochemical testing as well as SL characterization was performed. The by far best performance in all measurements granted the cell with the electrolyte containing TMSP. It provided a specific capacity of 23 mAh and a CE of 97 % after 50 cycles. In contrast to that, the cell with the base electrolyte only reached a CE of 80 %. Additionally, the cell containing TMSP provided a capacity loss of 9.89 % in self- discharge measurements. Thus, it is a promising additive to prevent self-discharge.

EIS measurements grant information about the interphase (SL and SEI) between electrolyte and electrodes. The cell containing TMSP exhibits the smallest impedance after the 1^{st} and 50^{th} cycle. In contrast to that all other cells containing additives provides a drastic increase in its impedance after the 50^{th} cycle.

All SL characterizations exhibit a similar result in comparison to the LNMO SL. Hence, the electrolyte degrades in a way similar to LNMO.

Further work should focus on the detection of gas evolution during cycling in half and full cells. Furthermore, the inorganic and organic compounds of the SL should be characterized to gain information of the amount of decomposed salt. Since the cell with the electrolyte containing TMSP provided by far the best electrochemical performance, this additive should be taken into account for further investigations.

4 Experimental Part

4.1 Preparation of LP30 with and without additives

All reagents, except glutaric anhydride and dimethyl carbonate, were purchased from TCI (branch: Tokyo; Japan; purity: SA: 95 %; PES: 98 %; TMSB: 97 %; TMSP: 96 %; EC: 99 %). Glutaric anhydride was purchased from Sigma Aldrich (branch: Steinheim, Germany; purity: 95 %) and dimethyl carbonate (DMC) from Alfa Aesar (branch: Karlsruhe, Germany; purity: 99 %), respectively. All preparations were performed in an argon filled Glove box with moisture and oxygen level below 1 ppm. EC was dissolved in DMC (1:1 (m/m) and 1 M of lithiumhexafluorophosphate ($LiPF_6$)) was added to the solution. When additives were used, 2 wt.% of GA, SA, PES, TMSP and TMSB were added to the electrolyte mixture.

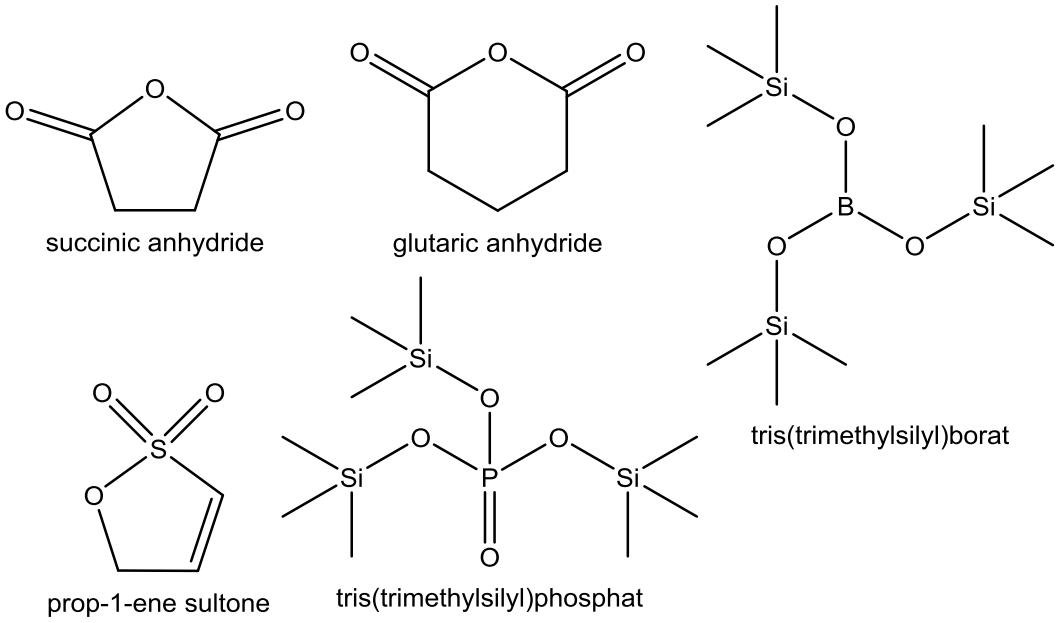

Figure 35: additives used in LP30 electrolyte

4.2 Preparation of electrodes

4.2.1 LNMO electrodes

Slurries were prepared from LNMO (gracious gift from Sergio Brutti; Department of Chemistry, University of Rome "La Sapienza", Rome, Italy[6]), polyvinylidendifluoride (PVDF, Kynar; branch: Colombes, France; purity: < 100 %), SuperP (Timcal; branch: Düsseldorf, Germany; purity: > 96 %) in NMP (abcr; branch: Karlsruhe, Germany; purity: 99 %).The composition of all electrodes was 80 % LNMO, 10 % PVDF and 10 % SuperP. The binder was dissolved in NMP via stirring and LNMO and conductive carbon black were added and stirred overnight. The resulting slurry was either casted on a 30 µm Al-foil (Roth; branch: Karlsruhe, Germany) with a gap size of 100 µm for the usage in Swagelok cells, or put on an

Al-mesh (diameter 37 mm) for OEMS cells. Subsequently, the foils/meshes were dried at 60 °C overnight and 10 mm electrodes were punched out of the foil. After drying at 120 °C under vacuum overnight the electrodes were weighed and dried again for 2 h at 120 °C under vacuum.

4.2.2 LCP electrodes

LCP was synthesized by S. Brutti et al. (Department of Chemistry, University of Rome "La Sapienza", Rome, Italy) by a solvo-thermal method.[91] Slurries and electrodes were prepared as described in the previous section for LNMO.

4.2.3 LFP electrodes

4.2.3.1 Delithation of $LiFePO_4$

LFP was a gracious gift from the group of Peter Bruce (School of Chemistry, University of St. Andrews, St. Andrews (UK)). For further usage as counter electrode LFP had to be delithated. For partial delithation, LFP (0.50 g; 3.17 mmol) was stirred with 12.5 mL of deionized H_2O to form a suspension. Glacial acetic acid (200 µL; 100 %; Merck; branch: Darmstadt, Germany; purity: 99.8 %) and hydrogen peroxide (500 µL; 30 %, Roth; branch: Karlsruhe, Germany, purity: 29 – 31 %) were added to 5 ml of deionized H_2O and then mixed with the suspension. The mixture was stirred for 2 h at RT and afterwards centrifuged at 3500 rpm for 5 min. The partly delithated LFP was washed with of deionized H_2O three times and dried at 60°C overnight. For complete delithation the powder (0.469 g) was added to 6.25 mL of deionized H_2O and stirred. Glacial acetic acid (200 µL; 100%) and hydrogen peroxide (500 µL; 30 %) were added to 2.5 ml of deionized H_2O and then added to the suspension. After 2 h the mixture was centrifuged and washed three times with of deionized H_2O. The grey powder was dried at 60°C overnight. For the determination of the degree of delithation an XRD was taken.

Yield: 454.1 mg of a grey powder

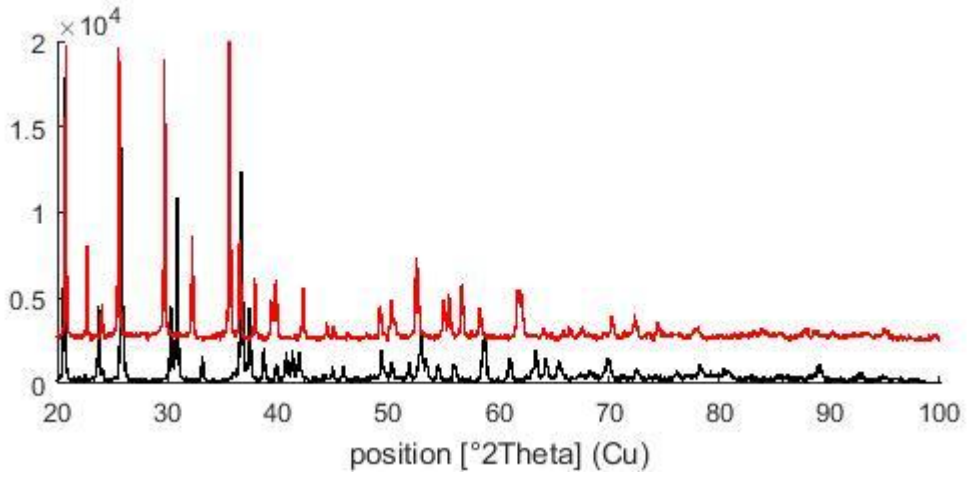

Figure 36: XRD of LFP (red) and delithiated LFP (black).

According to XRD data the powder was delithiated to 94 %.

4.2.3.2 Electrode preparation

Slurries and electrodes were prepared as described in section 5.2.1 for LNMO, except that the gap size for casting was 120 µm.

4.3 Cell assembly

4.3.1 Swagelok cells

All cells were assembled with a three electrode arrangement (LNMO (WE), Li (RE, CE)) in a Glovebox under Ar. 240 µl of electrolyte were used in each cell. A glass fiber separator (GF/F, Whatman; branch: Darmstadt, Germany) was used. The assembly of a Swagelok cell is shown in Figure 37 .

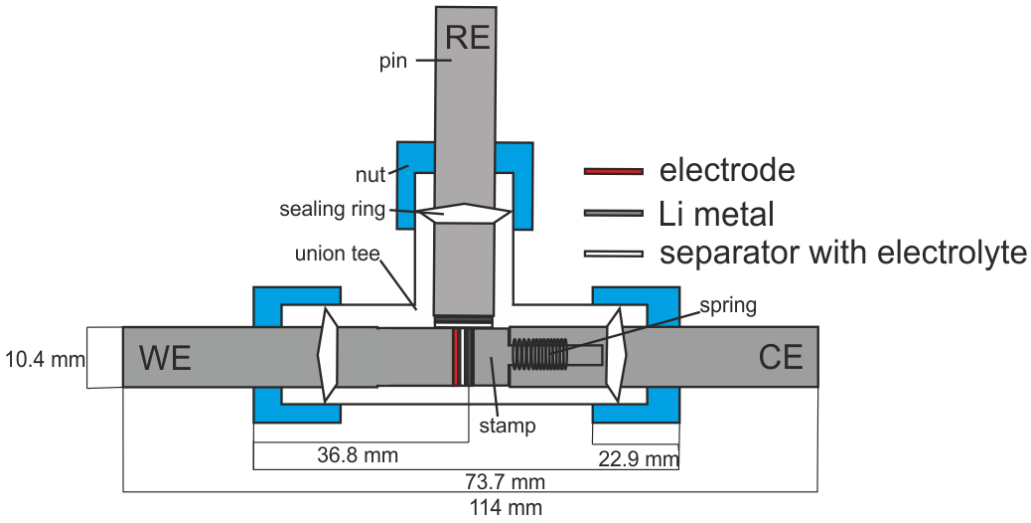

Figure 37: Sketch of a Swagelok cell. Used material for Union Tee PFA and for the pins Mangalloy steel.

4.3.2 Assembly of OEMS cell

The OEMS cell has a three electro configuration with LNMO on aluminum mesh as a working electrode (diameter 37 mm), a Cu wire with Li metal as reference electrode and delithiated LFP on aluminum foil (full cell) or Li metal on copper foil (half-cell) as counter electrode (diameter 38 mm). Glass fiber tissues (GF/F, 38 mm, Whatman) and polypropylene membranes (Celgard) were used as separators and LP30 (1:1 EC:DMC; 1 M $LiPF_6$) and 2 wt.% additive as electrolyte. The assembly of an OEMS cell is illustrated in Figure 38. A calibration was performed with different gases (Ar, O_2, CO_2, H_2, N_2, H_2O) using different mixtures.

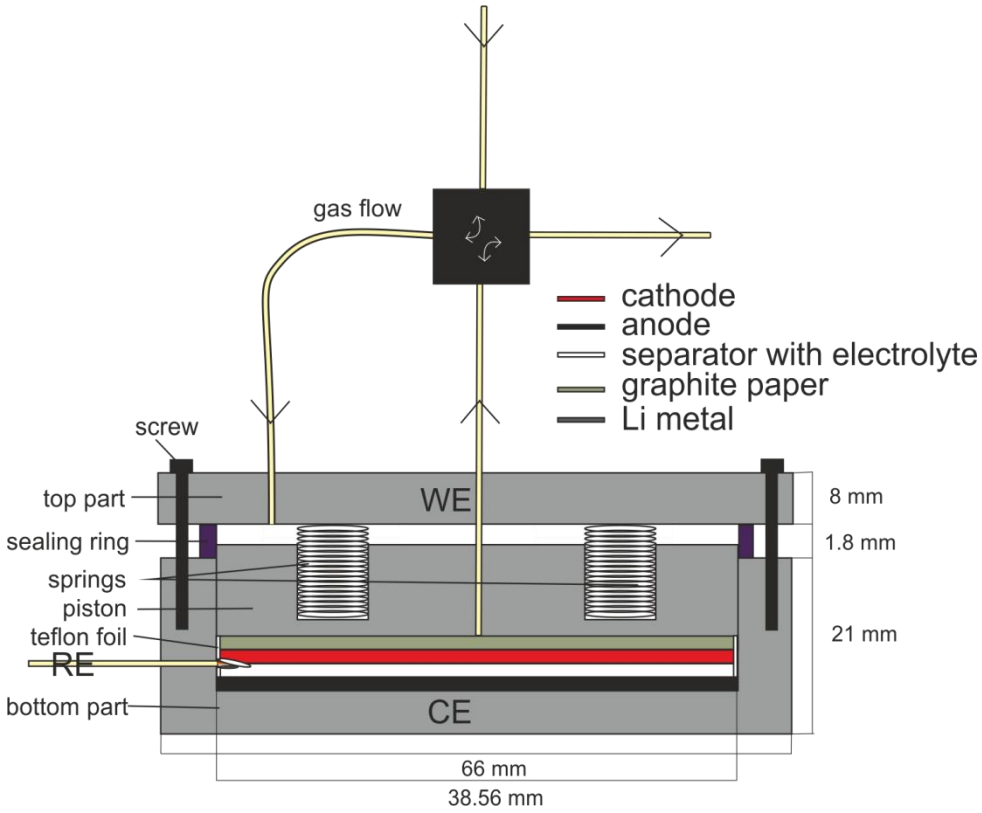

Figure 38: Sketch of an OEMS cell. Used materials are stainless steel and Teflon.

4.4 Measurements

4.4.1 Stability of the additives

The stability of the additives succinic anhydride (SA), glutaric anhydride (GA), prop-1-en sultone (PES), tris(trimethylsilyl)phosphate (TMSP) and tris(trimethylsilyl)borate (TMSB) were investigated by cyclic voltammetry (CV) on a SP-300 potentiostat/galvanostat (BioLogic). 1.5 ml electrolyte (acetonitrile; 0.1 M $LiClO_4$; 2 wt.% additive) was used for each measurement. A three electrode arrangement was prepared with LFP as reference and counter electrode and glassy carbon (diameter: 3 mm; CH instruments; Part Number: CHI104) (blank; with LNMO/SuperP and SuperP coating) as working electrode. The voltage range was chosen between 0 V – 2.5 V with a scan rate of 100 mV/s. Ferrocene was used as internal reference.

4.4.2 In-situ measurements

4.4.2.1 Cycling performance

BT - 2000 (Arbin) and a MPG-2 (BioLogic) potentiostats/galvanostats were used for cycling tests, respectively. The parameters were derived from similar experiments by Stefano Passerini's group (Institute of Physical Chemistry and MEET Battery Research Centre,

University of Muenster, Muenster, Germany).[19] The protocol included constant current charge at C/2 to 5.0 V and then a constant voltage step until the current drops to 1/10 of the charging current followed by a discharge at C/2 to 5.0 V (5x). Then the cells were left at OCV for 99 h, and cycled again under the same conditions (45x).

4.4.2.2 Cyclic Voltammetry and MS investigations

Cyclic voltammetry was carried out on a SP300 (BioLogic). The voltage range for LNMO and LCP was chosen between 3.95 – 5.00 V vs. Ref. with a sweep potential of 0.1 mV/s.

A TSU 065D (Balzers) quadrupole mass spectrometer with a turbomolecular pump (Pfeiffer) (backed by a membrane pump) was used for MS investigations. The gas flow (Ar) of the purge gas was 0.2 ml/min with a recording interval of 40 seconds.

4.4.2.3 Electrochemical Impedance Spectroscopy (EIS)

Electrochemical impedance spectroscopy (EIS) was carried out on a biologic workstation in the glovebox under Ar atmosphere. EIS measurements were conducted under potential control with a sinus amplitude of 20 mV in a frequency range of 7 MHz - 2.3 mHz for the cells with 50 charge/discharge cycles and 7 MHz – 32 mHz for those measured after the first cycle.

4.4.2.4 NMR and FTIR spectroscopy

After 50 cycles, the Swagelok cells were disassembled in a Glovebox under Ar atmosphere. The electrolyte and separator were washed with $CDCl_3$ directly into a NMR tube. After washing with DCM and drying in a vacuum chamber an FTIR of the electrode was taken. Finally, the electrodes and separators were washed with D_2O, respectively. A ^{1}H-NMR was taken of each $CDCl_3$ and D_2O sample.

References

1. Armand M, Tarascon J-M. Issues and challenges facing rechargeable lithium batteries. *Nature*. 2001;**414**:359-367.
2. Nagaura T. Development of rechargeable lithium batteries. II. Lithium ion rechargeable batteries. *Prog Batter Sol Cells*. 1991;**10**:209-226.
3. Ohzuku T, Makimura Y. Layered Lithium Insertion Material of LiNi1/2Mn1/2O2 : A Possible Alternative to LiCoO2 for Advanced Lithium-Ion Batteries. *Chem Lett*. 2001;**2**:744-745.
4. Huang H, Yin S-C, Nazar LF. Approaching Theoretical Capacity of LiFePO 4 at Room Temperature at High Rates. *Electrochem Solid-State Lett*. 2001;**4**:A170-A172.
5. Brutti S, Greco G, Reale P, Panero S. Insights about the irreversible capacity of LiNi0.5Mn1.5O4 cathode materials in lithium batteries. *Electrochim Acta*. 2013;**106**:483-493.
6. Chi LH, Dinh NN, Brutti S, Scrosati B. Synthesis, characterization and electrochemical properties of 4.8V LiNi0.5Mn1.5O4 cathode material in lithium-ion batteries. *Electrochim Acta*. 2010;**55**:5110-5116.
7. Manzi J, Vitucci FM, Paolone A, et al. Analysis of the self-discharge process in LiCoPO4 electrodes: Bulks. *Electrochim Acta*. 2015;**179**:604-610.
8. Choi N-S, Han J-G, Ha S-Y, Park I, Back C-K. Recent advances in the electrolytes for interfacial stability of high-voltage cathodes in lithium-ion batteries. *RSC Adv*. 2015;**5**:2732-2748.
9. Hu M, Pang X, Zhou Z. Recent progress in high-voltage lithium ion batteries. *J Power Sources*. 2013;**237**:229-242.
10. Aurbach D, Talyosef Y, Markovsky B, et al. Design of electrolyte solutions for Li and Li-ion batteries : a review. *Electrochim Acta*. 2004;**50**:247-254.
11. Ensling D, Stjerndahl M, Nytén A, Gustafsson T, Thomas JO. A comparative XPS surface study of Li2FeSiO4 /C cycled with LiTFSI- and LiPF 6 -based electrolytes. *J Mater Chem*. 2009;**19**:82-88.
12. Nishida T, Tashiro Y, Yamamoto M. Physical and electrochemical properties of 1-alkyl-3-methylimidazolium tetra uoroborate for electrolyte. *J Fluor Chem*. 2003;**120**:135-141.
13. Lee SY, Ueno K, Angell CA. Lithium salt solutions in mixed sulfone and sulfone-carbonate solvents: A walden plot analysis of the maximally conductive compositions. *J Phys Chem C*. 2012;**116**:23915-23920.
14. Ue M, Ida K, Mori S. Electrochemical Properties of Organic Liquid Electrolytes Based on Quaternary Onium Salts for Electrical Double-Layer Capacitors. *J Electrochem Soc*. 1994;**141**:2989.
15. Lee H, Choi S, Choi S, et al. SEI layer-forming additives for LiNi0.5Mn1.5O4/graphite 5 V Li-ion batteries. *Electrochem commun*. 2007;**9**:801-806.
16. Wang Z, Dupré N, Lajaunie L, et al. Effect of glutaric anhydride additive on the LiNi 0.4Mn 1.6O 4 electrode/electrolyte interface evolution: A MAS NMR and TEM/EELS study. *J Power Sources*. 2012;**215**:170-178.
17. Nie M, Xia J, Dahn JR. Development of Pyridine-Boron Trifluoride Electrolyte Additives for Lithium-Ion Batteries. *J Electrochem Soc*. 2015;**162**:A1186-A1195.
18. Yang L, Markmaitree T, Lucht BL. Inorganic additives for passivation of high voltage cathode materials. *J Power Sources*. 2011;**196**:2251-2254.
19. Tarnopolskiy V, Kalhoff J, Nádherná M, et al. Beneficial influence of succinic anhydride as electrolyte additive on the self-discharge of 5 v LiNi0.4Mn1.6O4 cathodes. *J Power Sources*. 2013;**236**:39-46.
20. He M, Boulet-Roblin L, Borel P, et al. Effects of Solvent, Lithium Salt, and Temperature on Stability of Carbonate-Based Electrolytes for 5.0 V LiNi0.5Mn1.5O4 Electrode s. *J Electrochem Soc*. 2015;**163**:A83-A89.
21. Streich D, Guéguen A, Mendez M, Chesneau F, Novák P, Berg EJ. Online Electrochemical Mass Spectrometry of High Energy Lithium Nickel Cobalt Manganese Oxide/Graphite Half- and Full-Cells with Ethylene Carbonate and Fluoroethylene

Carbonate Based Electrolytes. *J Electrochem Soc*. 2016;**163**:A964-A970.
22. Guéguen A, Streich D, He M, et al. Decomposition of LiPF 6 in High Energy Lithium-Ion Batteries Studied with Online Electrochemical Mass Spectrometry. *J Electrochem Soc*. 2016;**163**:A1095-A1100.
23. Marom R, Amalraj SF, Leifer N, Jacob D, Aurbach D. A review of advanced and practical lithium battery materials. *J Mater Chem*. 2011;**21**:9938.
24. Xu B, Qian D, Wang Z, Meng YS. Recent progress in cathode materials research for advanced lithium ion batteries. *Mater Sci Eng R Reports*. 2012;**73**:51-65.
25. Gong Z, Yang Y. Recent advances in the research of polyanion-type cathode materials for Li-ion batteries. *Energy Environ Sci*. 2011;**4**:3223-3242.
26. Padhi AK, Nanjundaswamy KS, Goodenough JB. Phospho-olivines as Positive-Electrode Materials for Rechargeable Lithium Batteries. *J Electrochem Soc*. 1997;**144**:1188-1194.
27. Amine, K., H. Yasuda MY. Olivine LiCoPO[sub 4] as 4.8 V Electrode Material for Lithium Batteries. *Electrochem Solid-State Lett*. 1999;**3**:178-179.
28. Zhou F, Cococcioni M, Kang K, Ceder G. The Li intercalation potential of LiMPO 4 and LiMSiO 4 olivines with M = Fe, Mn, Co, Ni. *Electrochem commun*. 2004;**6**:1144-1148.
29. Wolfenstine J, Allen J. Ni3+/Ni2+ redox potential in LiNiPO4. *J Power Sources*. 2005;**142**:389-390.
30. Rabanal ME, Gutierrez MC, Garcia-Alvarado F, Gonzalo EC, Arroyo-de Domphablo ME. Improved electrode characteristics of olivine – LiCoPO 4 processed by high energy milling. *J Power Sources*. 2006;**160**:523-528.
31. Liu J, Conry TE, Song X, Yang L, Doeff MM, Richardson TJ. Spherical nanoporous LiCoPO4 / C composites as high performance cathode materials for rechargeable lithium-ion batteries. *J Mater Chem*. 2011;**21**:9984-9987.
32. Han D, Kang Y, Yin R, Song M, Kwon H. Electrochemistry Communications Effects of Fe doping on the electrochemical performance of LiCoPO4 / C composites for high power-density cathode materials. *Electrochem commun*. 2009;**11**:137-140.
33. Ehrenberg H, Bramnik NN, Senyshyn A, Fuess H. Crystal and magnetic structures of electrochemically delithiated Li1-xCoPO4 phases. *Solid State Sci*. 2009;**11**:18-23.
34. Ellis BL, Makahnouk WRM, Makimura Y, Toghill K, Nazar LF. A multifunctional 3.5 V iron-based phosphate cathode for rechargeable batteries. *Nat Mater*. 2007;**6**:749-753.
35. Recham N, Chotard JN, Jumas JC, Laffont L, Armand M, Tarasco JM. Ionothermal synthesis of Li-based fluorophosphates electrodes. *Chem Mater*. 2010;**22**:1142-1148.
36. Ramesh TN, Lee KT, Ellis BL, Nazar LF. Tavorite Lithium Iron Fluorophosphate Cathode Materials: Phase Transition and Electrochemistry of LiFePO4F–Li2FePO4F. *Electrochem Solid-State Lett*. 2010;**13**:A43-A47.
37. Ellis BL, Ramesh TN, Rowan-Weetaluktuk WN, Ryan DH, Nazar LF. Solvothermal synthesis of electroactive lithium iron tavorites and structure of Li2FePO4F. *J Mater Chem*. 2012;**22**:4759.
38. Barker J, Saidi MY, Swoyer JL. Electrochemical Insertion Properties of the Novel Lithium Vanadium Fluorophosphate, LiVPO[sub 4]F. *J Electrochem Soc*. 2003;**150**:A1394-A1398.
39. Barker J, Gover RKB, Burns P, Bryan AJ. A Lithium-Ion Cell Based on Li4/3Ti5/3O4 and LiVPO4F. *Electrochem Solid-State Lett*. 2007;**10**:A130.
40. Barker J, Gover RKB, Burns P, Bryan a., Saidi MY, Swoyer JL. Performance Evaluation of Lithium Vanadium Fluorophosphate in Lithium Metal and Lithium-Ion Cells. *J Electrochem Soc*. 2005;**152**:A1776.
41. Zhou F, Zhao X, Dahn JR. Reactivity of charged LiVPO4F with 1 M LiPF6 EC:DEC electrolyte at high temperature as studied by accelerating rate calorimetry. *Electrochem commun*. 2009;**11**:589-591.
42. Okada S, Ueno M, Uebou Y, Yamaki JI. Fluoride phosphate Li2CoPO4F as a high-voltage cathode in Li-ion batteries. *J Power Sources*. 2005;**146**:565-569.
43. Nagahama M, Hasegawa N, Okada S. High Voltage Performances of Li2NiPO4F Cathode with Dinitrile-Based Electrolytes. *J Electrochem Soc*. 2010;**157**:A748-A752.
44. Sun Y-K, Myung S-T, Park B-C, Prakash J, Belharouak I, Amine K. High-energy

cathode material for long-life and safe lithium batteries. *Nat Mater*. 2009;**8**:320-324.
45. Oishi M, Fujimoto T, Takanashi Y, et al. Charge compensation mechanisms in Li1.16Ni0.15Co0.19Mn0.50O2 positive electrode material for Li-ion batteries analyzed by a combination of hard and soft X-ray absorption near edge structure. *J Power Sources*. 2013;**222**:45-51.
46. Johnson CS, Li N, Lefief C, Vaughey JT, Thackeray MM. Synthesis, Characterization and Electrochemistry of Lithium Battery Electrodes: x Li2MnO3(1−x)LiMn0.333Ni0.333Co0.333O2 (0 ≤ x ≤ 0.7). *Chem Mater*. 2008;**20**:6095-6106.
47. Wu Y, Vadivel Murugan A, Manthiram A. Surface Modification of High Capacity Layered Li[Li0.2Mn0.54Ni0.13Co0.13]O2 Cathodes by AlPO4. *J Electrochem Soc*. 2008;**155**:A635.
48. Yang M, Xu B, Cheng J, Pan C, Hwang B, Meng YS. Electronic , Structural , and Electrochemical Properties Spinel Materials. *Chem Mater*. 2011;**23**:2832-2841.
49. Alcantara R, Jaraba M, Lavela P, Tirado J, P. Structural and Electrochemical Study of New LiNi0. 5TixMn1.5-xO4 Spinel Oxides for 5-V. *Chem Mater*. 2003;**11**:2376-2382.
50. Zhong GB, Wang YY, Yu YQ, Chen CH. Electrochemical investigations of the LiNi0.45M0.10Mn1.45O4 (M = Fe, Co, Cr) 5V cathode materials for lithium ion batteries. *J Power Sources*. 2012;**205**:385-393.
51. Shiu J-J, Pang WK, Wu S. Preparation and characterization of spinel LiNi0.5−xMgxMn1.5O4 cathode materials via spray pyrolysis method. *J Power Sources*. 2013;**244**:35-42.
52. Liu D, Hamel-Paquet J, Trottier J, et al. Synthesis of pure phase disordered LiMn 1.45Cr0.1Ni0.45O4 by a post-annealing method. *J Power Sources*. 2012;**217**:400-406.
53. Arbizzani C, De Giorgio F, Porcarelli L, et al. Short communication Use of non-conventional electrolyte salt and additives in high-voltage graphite/LiNi0.4Mn1.6O4 batteries. *J Power Sources*. 2013;**238**:17-20.
54. Deng Y-F, Zhao S-X, Xu Y-H, Nan C-W. Effect of temperature of Li2O-Al2O3-TiO2-P2O5 solid-state electrolyte coating process on the performance of LiNi0.5Mn1.5O4 cathode materials. *J Mater Chem A*. 2014;**2**:18889-18897.
55. Cho J-H, Park J-H, Lee M-H, Song H-K, Lee S-Y. A polymer electrolyte-skinned active material strategy toward high-voltage lithium ion batteries: a polyimide-coated LiNi0.5Mn1.5O4 spinel cathode material case. *Energy Environ Sci*. 2012;**5**:7124.
56. Xu K. Electrolytes and interphases in Li-ion batteries and beyond. *Chem Rev*. 2014;**114**:11503-11618.
57. Goodenough JB, Kim Y. Challenges for Rechargeable Li Batteries. *Chem Mater*. 2010;**22**:587-603.
58. Ong SP, Andreussi O, Wu Y, Marzari N, Ceder G. Electrochemical Windows of Room-Temperature Ionic Liquids from Molecular Dynamics and Density Functional Theory Calculations. *Chem Mater*. 2011;**23**:2979-2986.
59. Howlett PC, Brack N, Hollenkamp a. F, Forsyth M, MacFarlane DR. 161 Characterization of the Lithium Surface in N-Methyl-N-alkylpyrrolidinium Bis(trifluoromethanesulfonyl)amide Room-Temperature Ionic Liquid Electrolytes. *J Electrochem Soc*. 2006;**153**:A595.
60. Howlett PC, MacFarlane DR, Hollenkamp AF. High Lithium Metal Cycling Efficiency in a Room-Temperature Ionic Liquid. *Electrochem Solid-State Lett*. 2004;**7**:A97.
61. Fernicola A, Croce F, Scrosati B, Watanabe T, Ohno H. LiTFSI-BEPyTFSI as an improved ionic liquid electrolyte for rechargeable lithium batteries. *J Power Sources*. 2007;**174**:342-348.
62. Seki S, Kobayashi Y, Miyashiro H, et al. Compatibility of N -Methyl- N -propylpyrrolidinium Cation Room-Temperature Ionic Liquid Electrolytes and Graphite Electrodes. *J Phys Chem C*. 2008;**112**:16708-16713.
63. Wu F, Zhu Q, Li L, Chen R, Chen S. A diisocyanate/sulfone binary electrolyte based on lithium difluoro(oxalate)borate for lithium batteries. *J Mater Chem A*. 2013;**1**:3659.
64. Watanabe Y, Kinoshita S, Wada S, Hoshino K, Morimoto H, Tobishima S. Electrochemical properties and lithium ion solvation behavior of sulfone-ester mixed

electrolytes for high-voltage rechargeable lithium cells. *J Power Sources*. 2008;**179**:770-779.
65. Li S, Zhao W, Cui X, et al. An improved method for synthesis of lithium difluoro(oxalato)borate and effects of sulfolane on the electrochemical performances of lithium-ion batteries. *Electrochim Acta*. 2013;**91**:282-292.
66. Abouimrane A, Belharouak I, Amine K. Sulfone-based electrolytes for high-voltage Li-ion batteries. *Electrochem commun*. 2009;**11**:1073-1076.
67. Abu-Lebdeh Y, Davidson I. New electrolytes based on glutaronitrile for high energy/power Li-ion batteries. *J Power Sources*. 2009;**189**:576-579.
68. Abu-Lebdeh Y, Davidson I. High-Voltage Electrolytes Based on Adiponitrile for Li-Ion Batteries. *J Electrochem Soc*. 2009;**156**:A60.
69. Moshkovich M, Cojocaru M, Gottlieb HE, Aurbach D. The study of the anodic stability of alkyl carbonate solutions by in situ FTIR spectroscopy , EQCM , NMR and MS. 2001;**497**:84-96.
70. Yu L, Liu H, Wang Y, et al. Preferential adsorption of solvents on the cathode surface of lithium ion batteries. *Angew Chemie - Int Ed*. 2013;**52**:5753-5756.
71. von Cresce A, Xu K. Electrolyte Additive in Support of 5 V Li Ion Chemistry. *J Electrochem Soc*. 2011;**158**:A337.
72. Xing L, Li W, Wang C, et al. Theoretical investigations on oxidative stability of solvents and oxidative decomposition mechanism of ethylene carbonate for lithium ion battery use. *J Phys Chem B*. 2009;**113**:16596-16602.
73. Yang L, Ravdel B, Lucht BL. Electrolyte Reactions with the Surface of High Voltage LiNi0.5Mn1.5O4 Cathodes for Lithium-Ion Batteries. *Electrochem Solid-State Lett*. 2010;**13**:A95.
74. Dedryvère R, Foix D, Franger S, Patoux S, Daniel L, Gonbeau D. Electrode/Electrolyte Interface Reactivity in High-Voltage Spinel LiMn 1.6 Ni 0.4 O 4 /Li 4 Ti 5 O 12 Lithium-Ion Battery. *J Phys Chem C*. 2010;**114**:10999-11008.
75. Murakami M, Yamashige H, Arai H, Uchimoto Y, Ogumi Z. Direct Evidence of LiF Formation at Electrode/Electrolyte Interface by Li-7 and F-19 Double-Resonance Solid-State NMR Spectroscopy. *Electrochem Solid State Lett*. 2011;**14**:A134-A137.
76. Bouayad H, Wang Z, Dupré N, et al. Improvement of electrode/electrolyte interfaces in high-voltage spinel lithium-ion batteries by using glutaric anhydride as electrolyte additive. *J Phys Chem C*. 2014;**118**:4634-4648.
77. Li B, Xu M, Li T, Li W, Hu S. Prop-1-ene-1,3-sultone as SEI formation additive in propylene carbonate-based electrolyte for lithium ion batteries. *Electrochem commun*. 2012;**17**:92-95.
78. Xia J, Aiken CP, Ma L, et al. Combinations of Ethylene Sulfite (ES) and Vinylene Carbonate (VC) as Electrolyte Additives in Li(Ni1/3Mn1/3Co1/3)O2/Graphite Pouch Cells. *J Electrochem Soc*. 2014;**161**:A1149-A1157.
79. Xu K. Tailoring Electrolyte Composition for LiBOB. *J Electrochem Soc*. 2008;**155**:A733.
80. Madec L, Ma L, Nelson KJ, et al. The Effects of a Ternary Electrolyte Additive System on the Electrode/Electrolyte Interfaces in High Voltage Li-Ion Cells. *J Electrochem Soc*. 2016;**163**:A1001-A1009.
81. Aravindan V, Cheah YL, Ling WC, Madhavi S. Effect of LiBOB Additive on the Electrochemical Performance of LiCoPO4. *J Electrochem Soc*. 2012;**159**:A1435-A1439.
82. Hu M, Wei J, Xing L, Zhou Z. Effect of lithium difluoro(oxalate)borate (LiDFOB) additive on the performance of high-voltage lithium-ion batteries. *J Appl Electrochem*. 2012;**42**:291-296.
83. Horino T, Tamada H, Kishimoto a., et al. High Voltage Stability of Interfacial Reaction at the LiMn2O4 Thin-Film Electrodes/Liquid Electrolytes with Boroxine Compounds. *J Electrochem Soc*. 2010;**157**:A677.
84. Burns JC, Xia X, Dahn JR. The Effect of Trimethoxyboroxine on Carbonaceous Negative Electrodes for Li-Ion Batteries. *J Electrochem Soc*. 2012;**160**:A383-A386.
85. Sharabi R, Markevich E, Fridman K, et al. Electrolyte solution for the improved cycling

performance of LiCoPO4/C composite cathodes. *Electrochem commun*. 2013;**28**:20-23.
86. Zuo X, Fan C, Liu J, Xiao X, Wu J, Nan J. Effect of tris(trimethylsilyl)borate on the high voltage capacity. *J Power Sources*. 2013;**229**:308-312.
87. Xu M, Liu Y, Li B, Li W, Li X, Hu S. Tris (pentafluorophenyl) phosphine: An electrolyte additive for high voltage Li-ion batteries. *Electrochem commun*. 2012;**18**:123-126.
88. Tan S, Zhang Z, Li YY, et al. Tris(hexafluoro-iso-propyl)phosphate as an SEI-Forming Additive on Improving the Electrochemical Performance of the Li[Li0.2Mn0.56Ni0.16Co0.08]O2 Cathode Material. *J Electrochem Soc*. 2013;**160**:A285-A292.
89. Yan G, Li X, Wang Z, Guo H, Wang C. Tris (trimethylsilyl) phosphate : A fi lm-forming additive for high voltage cathode material in lithium-ion batteries. *J Power Sources*. 2014;**248**:1306-1311.
90. Tasaki K, Goldberg A, Lian J-J, Walker M, Timmons A, Harris SJ. Solubility of Lithium Salts Formed on the Lithium-Ion Battery Negative Electrode Surface in Organic Solvents. *J Electrochem Soc*. 2009;**156**:A1019-A1027.
91. Brutti S, Manzi J, De Bonis A, et al. Controlled synthesis of LiCoPO4 by a solvo-thermal method at 220°C. *Mater Lett*. 2015;**145**:324-327.
92. Xue Y, Wang Z, Zheng L, et al. Investigation on preparation and performance of spinel LiNi0.5Mn1.5O4 with different microstructures for lithium-ion batteries. *Sci Rep*. 2015;**5**:13299.
93. Wang Y, Shao X, Xu H, et al. Facile synthesis of porous LiMn2O4 spheres as cathode materials for high-power lithium ion batteries. *J Power Sources*. 2013;**226**:140-148.
94. Younesi R, Christiansen AS, Scipioni R, et al. Analysis of the Interphase on Carbon Black Formed in High Voltage Batteries. *J Electrochem Soc*. 2015;**162**:A1289-A1296.
95. Uddin J. *Macro To Nano Spectroscopy*. InTech; 2012.
96. Manzi J, Curcio M, Brutti S. Structural and Morphological Tuning of LiCoPO4 Materials Synthesized by Solvo-Thermal Methods for Li-Cell Applications. *Nanomaterials*. 2015;**5**:2212-2230.